Crystallographic fabrics of omphacite, rutile and quartz in Vendée eclogites (Armorican Massif, France). Consequences for deformation mechanisms and regimes

Alexandra Mauler [a], Gaston Godard [b,*], Karsten Kunze [a]

[a]*Geologisches Institut, ETH-Zentrum, CH-8092 Zurich, Switzerland*
[b]*CNRS-FRE 2316, Laboratoire de Pétrologie Métamorphique, Université Paris 7, 4 place Jussieu,*
F-75252 Paris Cedex 05, France

Abstract

This study aims at further understanding of the mechanisms how lattice-preferred orientations (LPO) develop during deformation in the main eclogite minerals. Microstructures and textures of deformed eclogites from the Les Essarts complex (Western France) were investigated using optical microscopy and electron backscatter diffraction (EBSD) in the scanning electron microscope. Microfabric analyses of eclogite-facies minerals are used to identify their deformation mechanisms, which define the rheology at high-pressure metamorphic conditions. Mechanisms of intracrystalline deformation by dislocation movement (dislocation creep) result usually in a non-linear flow law (typically power law), while diffusive processes (diffusion creep) correspond to linear flow laws. General microstructural observations may suggest intracrystalline deformation (dislocation creep) of omphacite. The omphacite LPO vary between S- and L-type and correlate with oblate or prolate grain shape fabrics, respectively. Until now, these LPO types have not been understood by plasticity models based on dislocation glide on the known slip systems in clinopyroxene. An alternative interpretation is given in terms of anisotropic growth and dissolution, with grain boundary diffusion as the rate controlling process. There are further indications suggesting diffusion creep with concomitant anisotropic growth and dissolution as a main deformation mechanism in omphacite. In omphacite around a hollow garnet, crystallographic and shape fabrics align with the **c**[001] axes parallel to the grain elongations defining the mineral lineation, which rotates locally with the inferred flow direction. In this part, the grain sizes of omphacite and rutile are larger than in the surrounding matrix. The geometry of both the shape and crystallographic fabrics is interpreted to represent the local stress regime (directions and ratios of the principal stresses). The LPO of rutile duplicate the LPO of omphacite and a similar distinction between S- and L-type was used. Rutile deformation mechanisms probably involve dislocation creep as well as diffusion creep. Quartz mainly occurs as an interstitial phase with weak LPO patterns interpreted as random. No representative obliquity of the LPO in omphacite nor rutile with respect to foliation and lineation was observed to be used as potential shear sense criteria. However, the rutile LPO was slightly rotated relative to the omphacite LPO consistently in most

---

* Corresponding author.
E-mail address: godard@ipgp.jussieu.fr (G. Godard).

samples. The results suggest that diffusion processes are strongly involved in the deformation of eclogites. A linear flow law should be taken into account in tectonic models where eclogites are incorporated. © 2001 Elsevier Science B.V. All rights reserved.

1. Introduction

Eclogites and other high-pressure rocks that have been buried at depth greater than the normal thickness of the continental crust (30–40 km) form an important component of geophysical and geochemical models that are concerned with exhumation processes. Because little is known about the physical conditions of formation and deformation of eclogites, strong assumptions are made in such models concerning the deviatoric stresses sustained by eclogites at certain strain rates as well as their deformation mechanisms and rheology (Platt, 1993).

Further knowledge is needed about the deformation regimes (flattening or constriction, shear components) in eclogites, the dominant deformation mechanisms of the main eclogite-facies minerals and the stress magnitude sustained by eclogites. Attention has mainly been focused on omphacite, the framework-supporting mineral in eclogites. Garnet, the other major mineral, is generally assumed to behave as a rigid body during deformation. Indications about the dominant deformation mechanisms in naturally deformed rocks are mostly derived indirectly from observations of microstructures, from measurements of lattice preferred orientation (LPO) and from extrapolation of experimentally determined flow laws. The dominant deformation mechanisms define the rheology at high-pressure metamorphic conditions. Mechanisms of intracrystalline deformation by dislocation movement (dislocation creep) result usually in a non-linear flow law (typically power law), while diffusive processes (diffusion creep) correspond to linear flow laws. It was suggested (Buatier et al., 1991; Philippot and Van Roermund, 1992) that power law creep processes may be dominant in eclogites down to a pressure of 1.2–1.4 GPa and a temperature of 500–550 °C. Here we will discuss deformation in eclogites based on new LPO data of all main mineral phases in eclogites from the Les Essarts Complex (Western France).

In the LPO patterns most commonly observed in natural eclogite clinopyroxene, **c**[001] is preferentially oriented parallel to the lineation while **b**[010] is normal to the foliation plane. It is often observed that this pattern varies with the axis ratios of the shape fabric ellipsoid (e.g., Godard and Van Roermund, 1995). In strongly lineated samples, the maximum of **c**[001] forms a point maximum parallel to the lineation and **b**[010] spreads out in a great circle normal to the lineation (L-type fabric of Helmstaedt et al., 1972). In strongly foliated samples, the maximum of **b**[010] describes a point maximum normal to the foliation plane, while **c**[001] is dispersed within the foliation plane (S-type fabric of Helmstaedt et al., 1972). Recently, a temperature-dependent switch in dominant slip systems due to a space group transformation was also discussed as the cause of the L- to S-type transition (Brenker, 1998; Brenker et al., 1999).

The deformation processes leading to the S- and L-type fabrics are not fully understood. The question remains whether they are controlled by crystal plastic processes such as multiple dislocation glide and climb (Buatier et al., 1991; Boundy et al., 1992; Philippot and Van Roermund, 1992; Brenker, 1998; Brenker et al., 1999; Bascou et al., 2001) or if other mechanisms such as diffusion creep are strongly involved (Helmstaedt et al., 1972; Godard, 1988; Godard and Van Roermund, 1995).

Through extensive TEM investigations on experimentally deformed non-sodic clinopyroxenes, two intracrystalline deformation regimes have been recognized in clinopyroxene. At low temperatures and high strain rates, plastic strain is accommodated by mechanical twinning on [**c**] (100) and [**a**] (001) and by dislocation glide on the [**c**] (100) slip system (Raleigh and Talbot, 1967; Avé Lallemant, 1978; Kollé and Blacic, 1983; Kirby and Kronenberg, 1984; Boland and Tullis, 1985). At high temperatures ($T > 500$ °C), multiple slip occurs involving the slip systems [**c**] (100), $1/2\langle \mathbf{a} \pm \mathbf{b}\rangle$ {110}, [**c**] {110}, [**a**]

(010), [**b**] (100) and [**a** + **c**] (010) (Boland and Tullis, 1985; Ingrin et al., 1992). According to Ingrin et al. (1991) and Raterron et al. (1994), [**c**] (100) is the easiest slip system at intermediate temperature, while $1/2\langle \mathbf{a} \pm \mathbf{b} \rangle$ {110} and [**c**] {110} dominate at high temperature ($T = 800$ °C). As [**c**] (010) has not been reported as a dominant slip system in clinopyroxene, the S- and L-type preferred orientations cannot be explained by "easy slip" on this slip system. However, according to numerical modeling of LPO development by Bascou et al. (2001), the typical preferred orientations may well result from dislocation glide on the dominant slip systems [**c**] (100), $1/2\langle \mathbf{a} \pm \mathbf{b} \rangle$ {110} and [**c**] {110} and several other systems.

Abalos (1997) reported a small obliquity of the omphacite LPO with respect to the macroscopic foliation and lineation in eclogites from Cabo Ortegal (NW Spain). This obliquity consists of a $6°–8°$ rotation of the crystallographic orientation ellipsoid of omphacite about the intermediate reference axis (normal to lineation within foliation) with the sense of shear. Abalos (1997) attributed the obliqueness in the LPO to non-coaxial deformation components in eclogites in addition to any flattening or constriction strain. As the structural reference frame *XYZ* (given by foliation and lineation) is often difficult to be precisely defined, an error of at least $5°$ must be assumed for the external reference orientation. So far, oblique omphacite LPO have not been confirmed to be consistent.

In most eclogites, quartz and rutile are present in minor proportions only (up to a few volume percent). For this reason, their roles in eclogites have received little attention, although they could provide information not carried by omphacite, e.g. about the sense of shear or about paleopiezometry in eclogites. Only one quartz fabric was reported earlier from eclogites (Binns, 1967), and the measured **c**-axis distribution did not show any preferred orientations. In the same study, Binns concluded from qualitative observations that the rutile **c**-axes were preferentially oriented parallel to the lineation. Godard (1981) reported a preferred orientation of rutile with the **c**-axes lying in the foliation plane. Asymmetric patterns of **c**- and **a**-axes of quartz have frequently been used as reliable shear sense indicators in gneisses or quartzites (Schmid, 1982; Mainprice et al., 1986; Schmid and Casey, 1986; Fliervoet et al., 1997). Quartz and rutile

LPO might potentially be used to deduce the sense of shear in eclogites in a similar way.

There are several reasons for the lack of studies on complete fabrics in eclogites. Microfabric analysis of omphacite using the universal stage is tedious, time-consuming and prone to measurement errors. Only **c**-axes can be measured optically on rutile and quartz, while the cubic symmetry of garnet does not allow optical studies in principle. Conventional X-ray texture goniometry is not feasible because of many overlapping diffraction peaks of the different mineral phases and because of large grain sizes, and neutron diffraction facilities are rare. With the development of the new technique of electron backscatter diffraction (EBSD), the number of microfabric studies on experimentally and naturally deformed clinopyroxenes and garnets has significantly increased (Weber, 1997; Brenker, 1998; Mauler et al., 1998; Brenker et al., 1999; Daniel et al., 1999; Prior et al., 2000; Spiess et al., 2001; Kleinschrodt and McGrew, 2000; Mauler et al., 2000a,b). EBSD is a scanning electron microscope (SEM) technique to determine the complete lattice orientation of individual grains or subgrains with a spatial resolution of 1 μm and with an absolute angular resolution of $1–2°$ (Venables and Harland, 1973; Dingley et al., 1987). Automated acquisition and analysis of EBSD patterns allow rapid measurements of a large number of orientations on a polished specimen surface (about $1–5$ s per pattern). In principle it is applicable to polycrystalline solids of any crystal symmetry including optically isotropic and opaque minerals. Diffraction patterns were recently documented (Dingley et al., 1995) and indexed for several minerals including garnet, quartz (Lloyd et al., 1987; Kunze et al., 1994a), carbonates (Kunze et al., 1994b; Leiss and Barber, 1999), oxides (like rutile), sulfides (Boyle et al., 1998), plagioclase (Prior and Wheeler, 1999), omphacite (Brenker, 1998; Mauler et al., 1998) and olivine (Fliervoet et al., 1999). Prior et al. (1999) have recently reviewed the application of EBSD to rocks.

This study presents a petrostructural analysis of 20 eclogite samples from the Les Essarts Unit in the Vendée (Armorican Massif, Western France). Godard (1981, 1988) and Godard and Van Roermund (1995) have previously studied the petrology and some aspects of the LPO in these rocks. Now, the complete LPO of omphacite, rutile and quartz were measured

using EBSD to investigate fabric relationships between the different minerals on a large sample basis. The new data present a reliable set to characterize deformation-induced microfabrics of omphacite, rutile and quartz with relation to some of the fundamental deformation parameters occurring in eclogites and with respect to their rheology.

2. Geological setting and sample description

2.1. Geological setting

The studied eclogites belong to the Les Essarts high-pressure unit located near Nantes (Western France), which stretches right across the Vendée in a northwest–southeast direction (Fig. 1). This unit occurs between two late-Hercynian tectonic lineaments, namely the Vendée coal belt and the Sainte-Pazanne-Mervent lineament (Fig. 2; Godard, 2001). Eclogites and associated rocks form several km-long lenses that are stretched and slightly boudinaged within the surrounding gneisses. From the macroscopic dimensions of the lenses, high strain deformation is inferred in the eclogite bodies. These lenses, almost subvertical and parallel to foliation, are composed of eclogite, amphibolite derived from eclogite, ortho-leptynite and silicified serpentinite (birbirite) (Fig. 2). The surrounding rocks are ortho- and paragneisses. They are highly foliated and rich in white mica so they resemble micaschists. Nevertheless, they frequently show evidence of a gneissic paragenesis with biotite, garnet, plagioclase, quartz and microcline. Evidence of a high-pressure metamorphism has been observed in these rocks (garnet coronas, albite pseudomorphs after jadeite: Godard, 2001). Foliation (120 NE 80 on average) and lineation (305 NW 20 on average) in the gneisses are parallel to the syn-eclogite-facies foliation and lineation in the
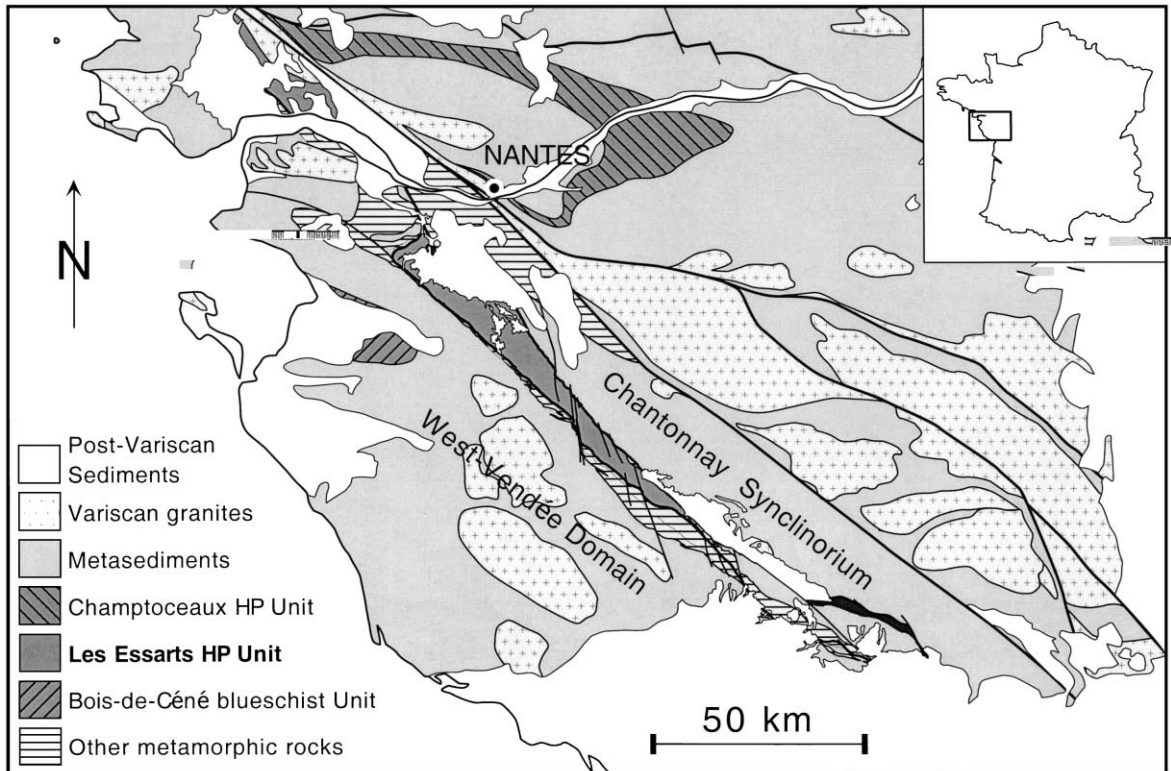

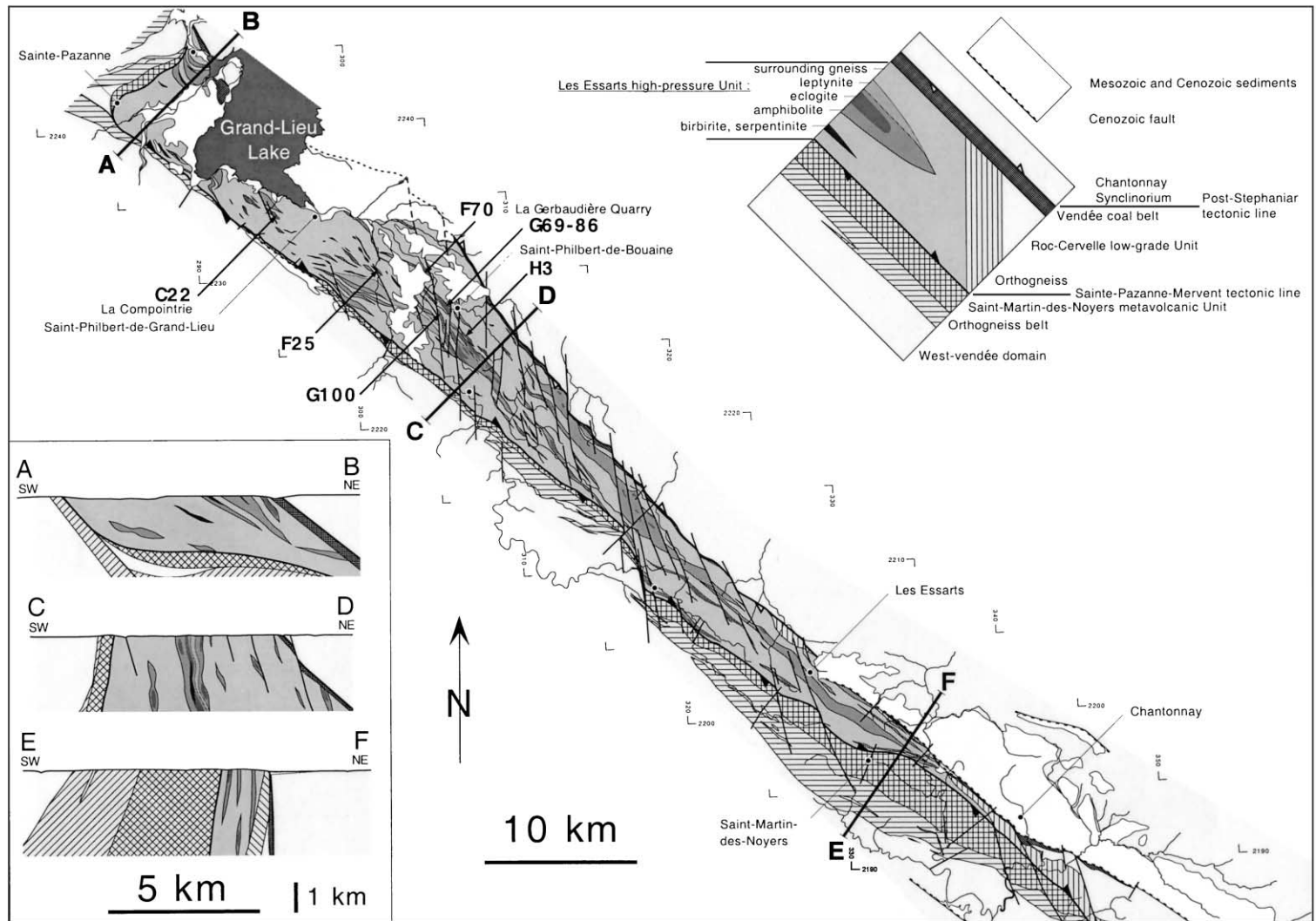Fig. 1. Regional geological map of the Vendée (Southern Armorican Massif, Western France).

Fig. 2. Geological map of Les Essarts Complex (after Godard, 2001). Coordinate system: Lambert II extended grid reference. Sample locations: C22 = 47°02′20″N–1°40′34″W; F25 = 47°00′32″N–1°35′22″W; F70 = 47°00′32″N–1°32′58″W; G69–80: see Fig. 3a; G100 = 46°59′10″N–1°31′16″W; H3 = 46°58′02″N–1°30′36″W.
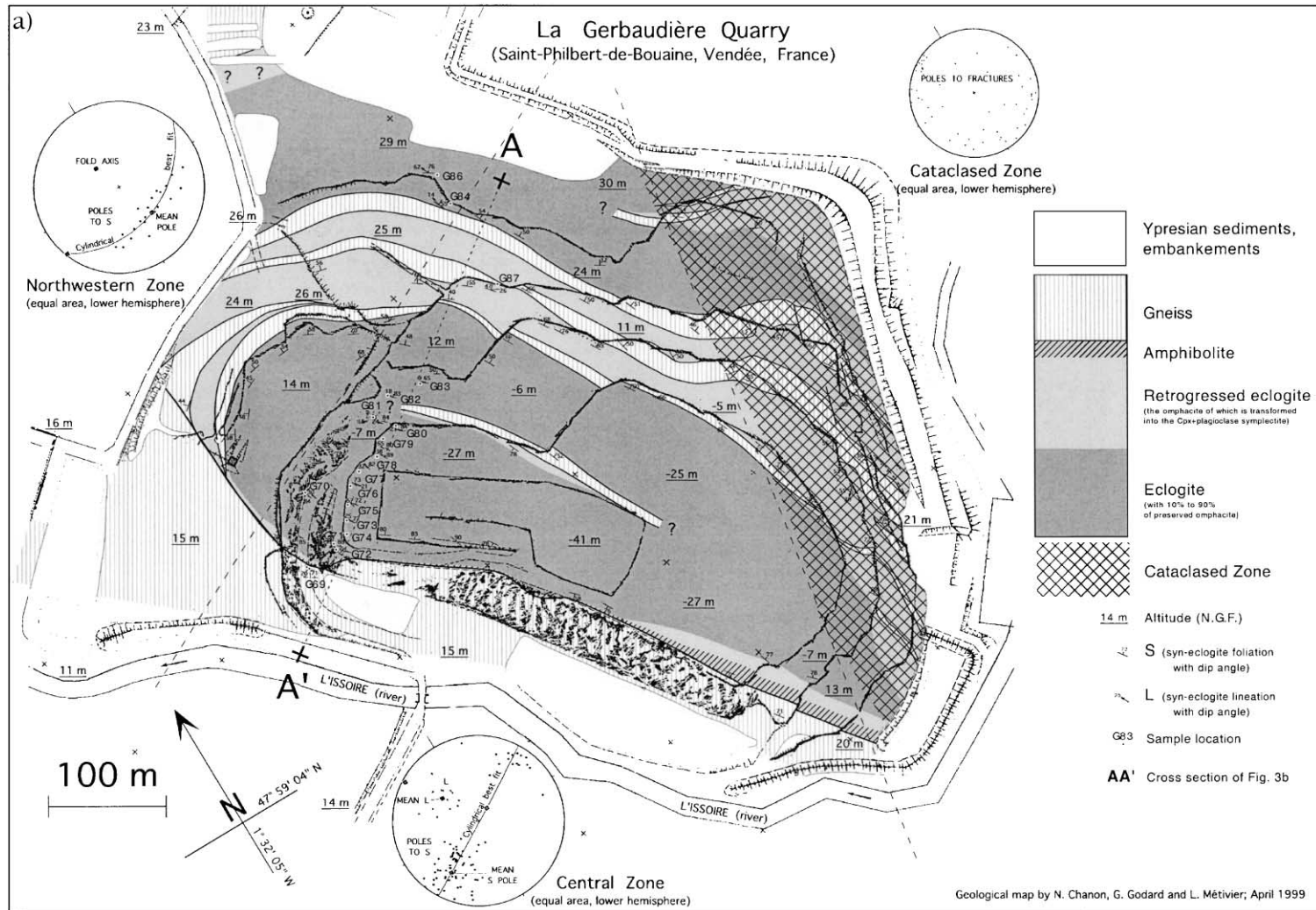
Fig. 3. Map and cross-section of the La Gerbaudière quarry in 1999. (a) Geological map of the quarry (after Godard, 2001). (b) Cross-section through the quarry along AA′. The sample positions and dip of foliations are shown.
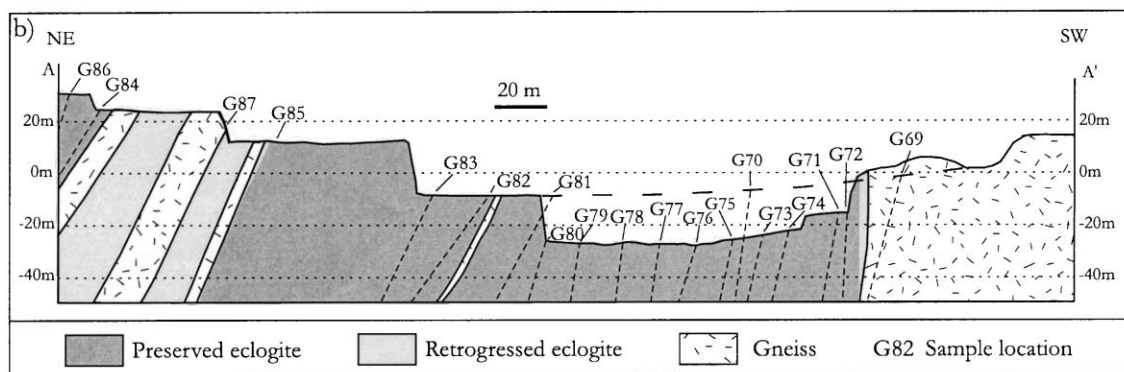
Fig. 3 (*continued*).

eclogites. Therefore, the gneisses seem to have undergone the same syn-eclogite-facies deformation event as the eclogite.

The geochemical features of the eclogites indicate an oceanic origin of their protolith. It has been proposed that they represent a fragment of a metamorphosed old oceanic crust (e.g., Montigny and Allègre, 1974; Godard, 1983, 1988). Moreover, the pre-eclogite parageneses and O isotope compositions are typical of an altered oceanic crust (Godard, 2001). However, the surrounding ortho- and paragneisses clearly belonged to a continental crust. They show evidence for a high-*T* orogenic cycle that had preceded the high-*P* metamorphism (former cordierite migmatitic paragneisses subsequently eclogitised). Therefore, Godard (2001) interprets the Les Essarts Unit as a possible tectonic melange of pre-Hercynian continental and oceanic crusts that were eclogitised during an eo-Variscan subduction and subsequently incorporated into the Hercynian orogenic belt.

2.2. Sample location and description

Most of the samples (G_{xx}) were taken in the La Gerbaudière eclogite quarry (Fig. 3). The other samples were found in different lenses distributed throughout Les Essarts Unit (Fig. 2). The foliation in the Les Essarts Unit is almost subvertical, while the stretching lineation is slightly dipping towards NW. Foliations in eclogite and gneiss are similar. Where the contact between eclogite and gneiss is visible, these structures seem to be parallel in both rocks,

suggesting that they deformed simultaneously. Strong unconformities between the two rocks occur rarely, like in the northwestern end of the La Gerbaudière quarry (Fig. 3a). Such unconformity is certainly due to a difference in rheology between eclogite and gneiss, which produced a boudinage effect. Some several meter thick levels of paragneiss are occasionally interbedded within the eclogite (e.g., La Gerbaudière quarry: Fig. 3). This gneiss is mainly made of quartz + plagioclase + biotite + garnet. K-feldspar is not abundant. Leucosomes seldom occur, indicating an incipient migmatisation. The foliation in the gneiss is parallel and apparently contemporaneous with the syn-eclogite foliation of the neighbouring eclogite. Evidence of high-*P* metamorphism is generally lacking in those gneisses, which suggests a late reequilibration, probably during migmatisation.

2.3. Petrology

The petrology of Vendée eclogites was described by Godard (1981, 1988). Their primary high-pressure mineral assemblage is omphacite + garnet + rutile ± quartz ± kyanite ± zoisite ± magnesio-hornblende. Thermo-barometric estimations gave $P > 1.3$ GPa and $T = 650$ to $750\,°C$. An age of 440 Ma was proposed by Peucat et al. (1981) for the eclogitisation.

The eclogite samples studied here contain the high-pressure mineral assemblage omphacite + garnet + quartz + rutile + zoisite. Typically, samples contain 45–55% omphacite, 30–40% garnet, 2–7% quartz and 1–3% rutile (in vol.%). Omphacite compositions

are fairly similar in all samples ($X_{Mg} = 0.79 - 0.84$, $X_{Jd} = 0.28 - 0.37$, $X_{Aeg} = 0.00 - 0.05$: Fig. 4) and very homogeneous within each sample ($1\sigma_{X_{Jd}} = 0.007 - 0.013$). The latter observation suggests that the plastic deformation destroyed any zonation in omphacite, whereas the garnet crystals preserved their strong zonation and subhedral shapes, as they behaved rigidly. Retrogression is indicated by the presence of green amphibole and plagioclase-clinopyroxene symplectite developed along omphacite grain boundaries. Amphibolitisation always affects the margins of the eclogite lenses (e.g., La Gerbaudière quarry: Fig. 3). When observed in eclogite, retrogression was static, without apparent deformation. The foliation in amphibolite is subparallel to but more scattered than that in eclogite, suggesting that the stress field was rather constant during retrogression.

2.4. Microstructures

The foliation (S) in the eclogite is marked by the shape preferred orientation (SPO) of omphacite (Figs. 5 and 6). Alternating thin layers with variations in garnet grain size and in mineral proportions, particularly amphibole-rich microlayers (Fig. 5a), are parallel to this foliation. Elongated omphacite crystals define a more or less pronounced stretching lineation (L) depending on the intensity and type of the shape fabric. Most omphacite grains have straight boundaries and sharp extinction with few visible intracrystalline defects. Some omphacite grains show characteristic features of intracrystalline deformation like deformation bands, undulous extinction and subgrains elongated parallel to the long axis of the grains. They are typically interpreted as evidence for dislocation creep. TEM observations on a sample originating from the quarry (sample G10 of Godard and Van Roermund, 1995) revealed dislocation glide to be active on the slip systems [001](100), $\langle 110 \rangle \{\bar{1}10\}$ and [001]{110}. A few deformation twins are unevenly present and only observed in cm-scale omphacite crystals (Godard, 1988). Deformation structures in omphacite are postdated by the post-eclogite retrogressive minerals that are clearly not elongated parallel to the foliation. The symplectite after omphacite, for example, is made of a fine association of clinopyroxene + plagioclase, which is expected to be unable to survive a strong deformation.

Garnet occurs as large euhedral crystals, with sizes up to several millimetres. They contain mineral inclusions, mainly quartz, amphibole, zoisite and rutile. In some eclogites, these inclusions in garnet define trails,
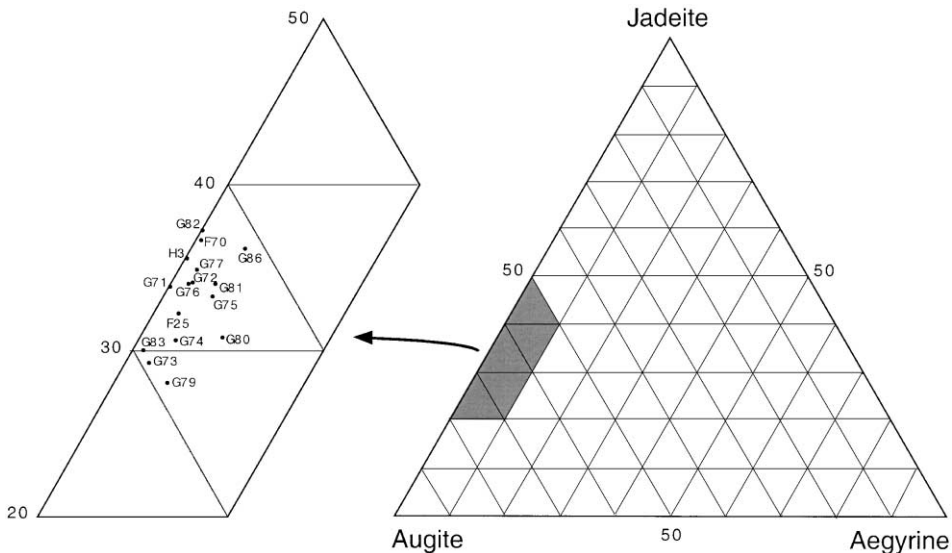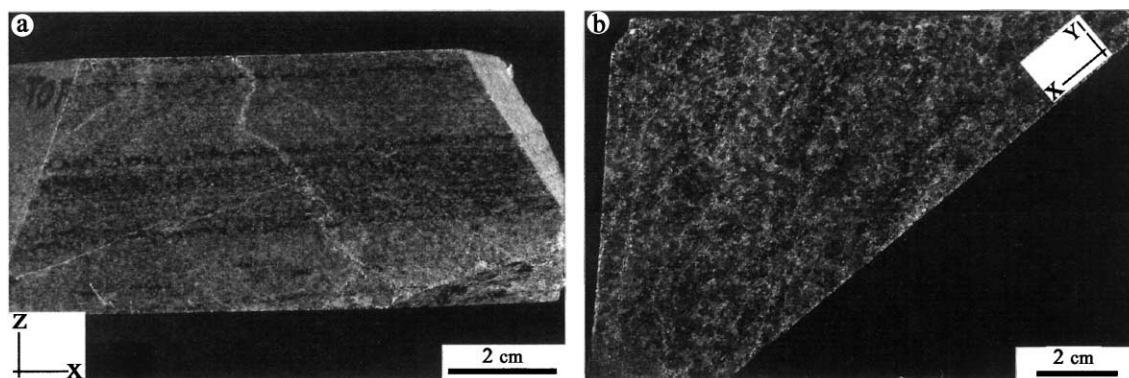

Fig. 4. Omphacite compositions.

Fig. 5. Hand specimen of eclogite sample G80: (a) *XZ* section: parallel to lineation and normal to foliation. (b) *XY* section: parallel to foliation and lineation.

which are interpreted as relics of a pre- or eo-eclogite foliation (Godard, 1988). Their orientation varies from garnet to garnet showing that garnets rotated passively during subsequent deformation. In some other samples, broken fragments of garnet crystals are dispersed in the omphacite matrix, indicating a rigid behaviour of garnet.

Rutile generally occurs as polycrystalline ribbons or individual grains within the omphacite matrix or between omphacite and garnet (Fig. 7b). It is often associated to ilmenite (Fig. 7c). Grain diameter ranges over from approximately 30–300 μm, with an average size around 100 μm. Grains are elongated subparallel to foliation and lineation and have commonly the shape of subhedral to anhedral prisms with average aspect ratio in the *XZ* sections around 2.5:1. In the *XY* sections, the aspect ratio is close to 1.5:1. Grain boundaries are straight to curved. The larger crystals are often twinned and contain subgrains, while the smaller grains are generally free of visible strain-induced defects (Fig. 7d–f).

Quartz occurs as irregularly shaped crystals, clustered to form polygranular aggregates. The grains are large and contain some subgrains but no further evidence of internal deformation (Fig. 7a). Grain boundaries between quartz grains are generally straight.

In the gneiss samples, quartz shows undulous extinction, deformation bands and subgrains, characteristic for intracrystalline deformation. New equant recrystallized grains are present. Plagioclase grains display abundant twins. Quartz–quartz and plagio-clase–quartz grain boundaries are strongly curved to lobate.

3. Analytical technique

3.1. Orientation measurements

Lattice preferred orientation (LPO) of omphacite, rutile and quartz were obtained from individual orientation measurements by EBSD (see Appendix A). The orientations from the various minerals in each sample were all measured during the same SEM session so that the external reference frame is perfectly identical for the LPO of the different minerals in the same sample. The reference frame (*XYZ*) was defined from precise positions of foliation and lineation based on the grain shape fabric, which was determined from the elongation of 100 omphacite grains in the *XZ* and *XY* sections, respectively (*X* = lineation, *XY* = foliation plane normal to *Z*). The measured pole figures were oriented with *XZ* in the drawing plane, such that the lineation is horizontal and the normal to the foliation is vertical.

LPO of omphacite and rutile were measured on all 20 eclogite samples. Quartz LPO were measured on 11 eclogite samples from the La Gerbaudière quarry (G72, G73, G75, G76, G78, G79, G81, G82, G83) and from two other eclogite lenses distributed in the Les Essarts Unit (F70, H3). Additionally, the LPO of quartz in two gneiss samples (G69 and G87) were studied, which
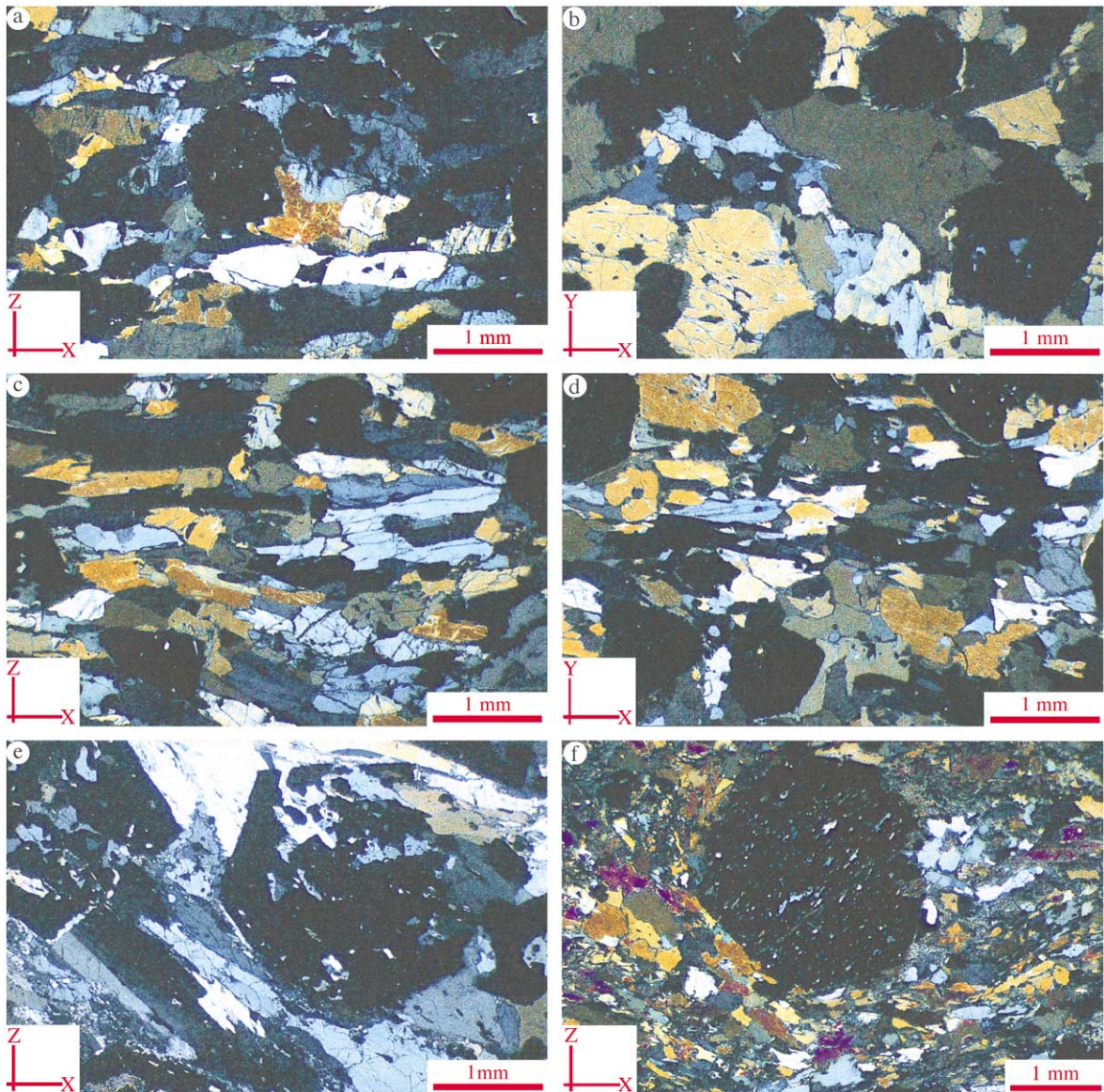
Fig. 6. Optical micrographs of the studied eclogites (crossed polarizers) and microstructures of omphacite: (a) S-type eclogite sample G81, section *XZ*. (b) S-type eclogite sample G81, section *XY*. (c) L-type eclogite sample G100, section *XZ*. (d) L-type eclogite sample G100, section *XY*. (e) Broken hollow garnet and deformed omphacite with strongly elongated subgrains (sample F25 section *XZ*). (f) Flow of omphacite wrapping around garnet (sample J23 section *XZ*). The omphacite grain size is larger in the garnet pressure shadows. Inclusions of quartz in the garnet are aligned.

were sampled close to the contact between the eclogite lens of the quarry and the surrounding rocks (Fig. 3).

Orientation distributions in pole figures and inverse pole figures were obtained using the software package Beartex (Wenk et al., 1998). The orientation distribu-

tion function (ODF) was calculated from the individual orientations using a Gaussian bell curve smoothing width of 30°. The strength of the texture was expressed by the texture index J calculated as the mean square value of the ODF (Bunge, 1982). A random LPO
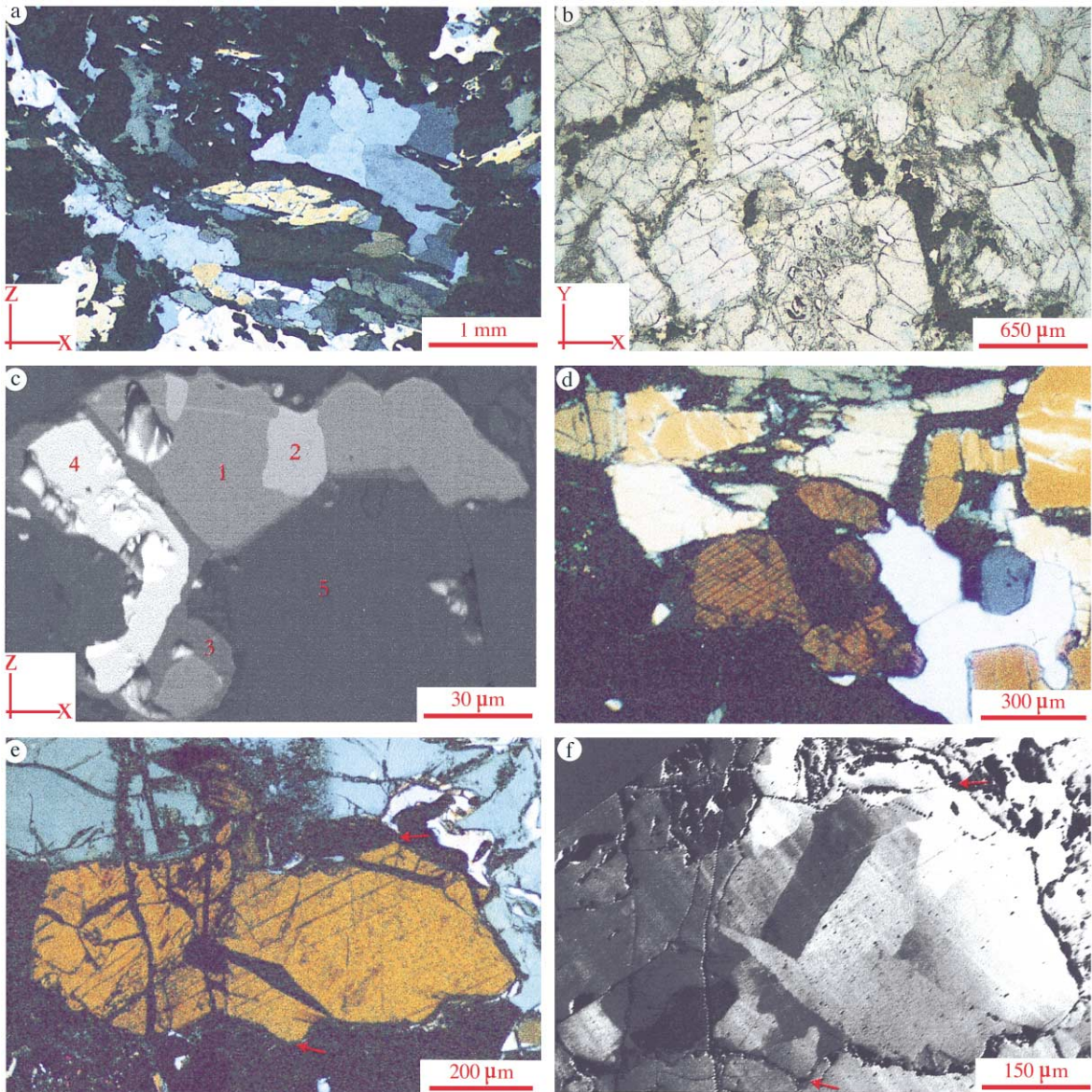
Fig. 7. Microstructures of quartz and rutile in the studied eclogites: (a) Optical micrographs of deformation features in quartz (crossed polarizers). The large quartz grains in the aggregate do not present any intracrystalline deformation structures; grain boundaries are nearly equilibrated (sample F25). (b) Optical micrographs showing the occurrence of rutile as ribbons of small grains between garnet and omphacite grains (sample G79). (c) SEM backscatter electron image of the common rutile association. 1. rutile, 2. ilmenite, 3. late sphene corona, 4. pyrite, 5. Omphacite (sample G80). (d) Optical micrograph of a rutile grain with two activated twin planes (sample G74). (e) Optical micrograph of a small aggregate of rutile grains (sample G77). (f) SEM orientation contrast of part of the same rutile grains as in (e) showing zones of small misorientations in one single grains, not visible in the optical micrograph.

would have constant ODF and pole figure values equal to 1 and therefore a texture index of 1, whereas for an infinitely sharp texture (single crystal), the texture index approaches infinity. With the applied smoothing width of $30°$, the maximum J is equal to 79.4 for a single orientation of monoclinic crystal symmetry.
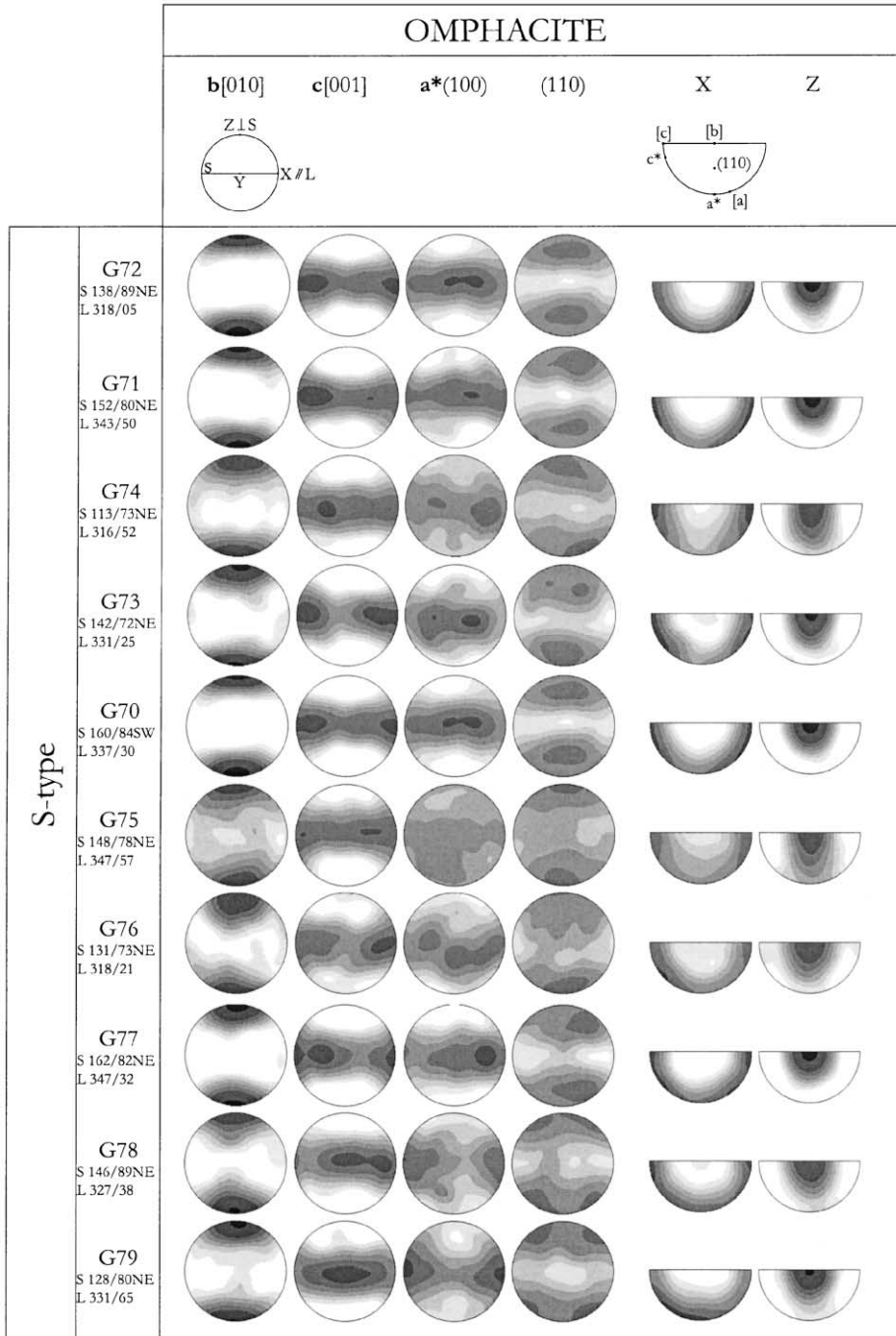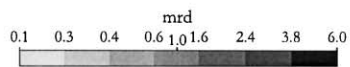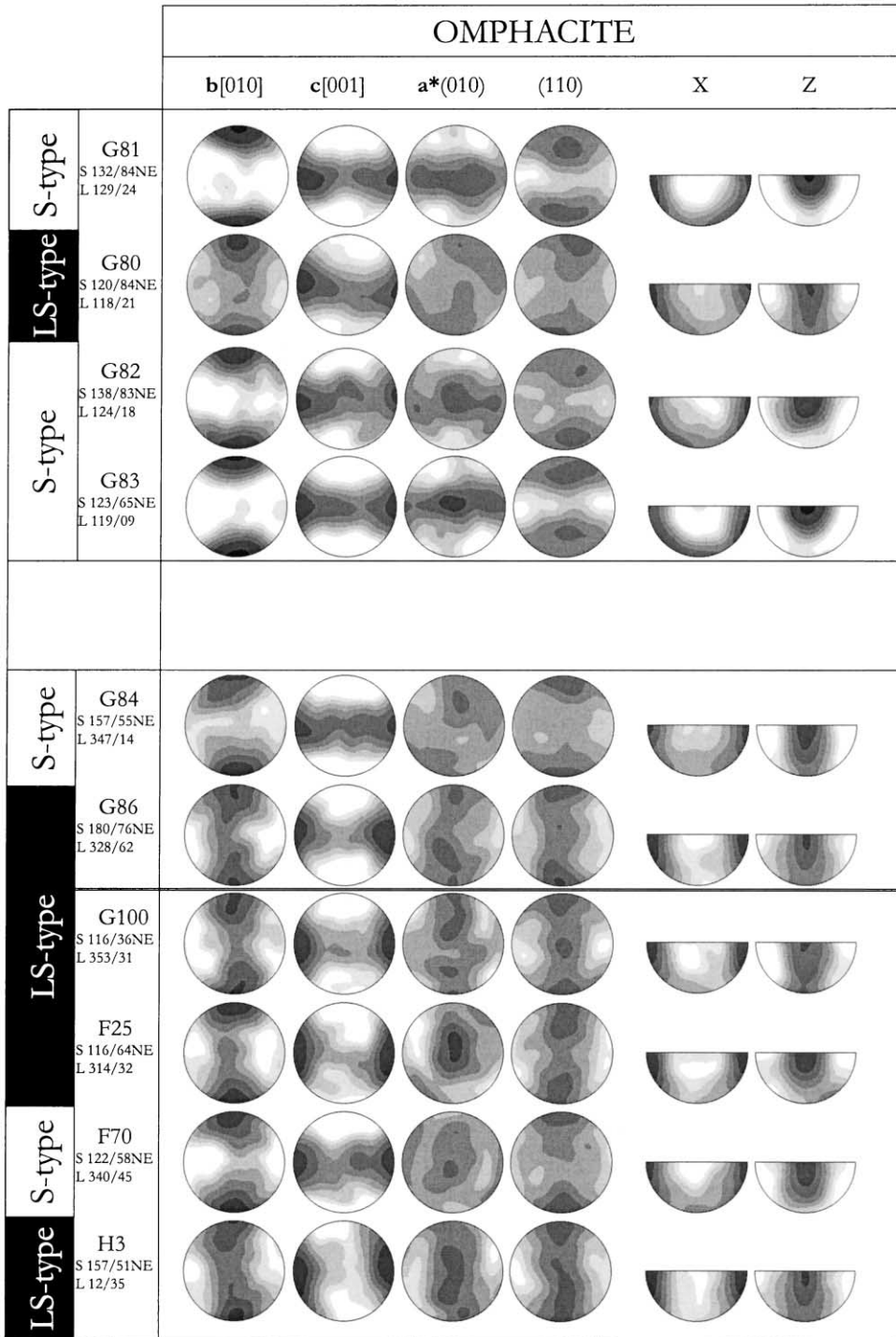
3.2. Eigenvalues and eigenvectors

The main features of each pole figure were characterized by eigenvalues and eigenvectors of the corresponding orientation ellipsoid (mathematically, the second-order moments of the distribution). A direction in three-dimensional space is a vector **v** with unit length, which can be represented by three direction cosines, taken as normalized Cartesian coordinates (v_1, v_2, v_3). For any single direction, the 3×3 symmetric covariance matrix $\{v_i v_k\}$ (with $i, k = 1, 2, 3$) of the direction cosines has the eigenvalues 1, 0, 0, and the three corresponding eigenvectors are, respectively, parallel and perpendicular to that direction. This corresponds to an orientation ellipsoid that is extremely pencil-shaped. For a distribution of many directions, the mean covariance matrix results from the weighted average of $\{v_i v_k\}$ over all directions corresponding to an average orientation ellipsoid. Diagonalization results in eigenvalues $e_1 \geq e_2 \geq e_3$ and eigenvectors $\upsilon_1, \upsilon_2, \upsilon_3$ characteristic for that distribution. Due to pole figure normalization the eigenvalues are normalized to $e_1 + e_2 + e_3 = 1$. The eigenvalues represent the strength of the distribution in the direction of the corresponding eigenvector, which is either the best-fit axis υ_1 of the distribution, the vector υ_2 perpendicular to the best-fit axis in the best-fit great circle, or the pole υ_3 to the best-fit great circle. Procedures for eigenvalues and eigenvector calculations were included as a subroutine in the Beartex package (Wenk et al., 1998) based on second-order harmonic coefficients (Bunge, 1982). A triangular presentation of the eigenvalues employs the indices *point* $(P = e_1 - e_2)$, *girdle* $(G = 2*(e_2 - e_3))$ and *random* $(R = 3*e_3)$ with $P + G + R = 1$, as introduced by Woodcock (1977) or Vollmer (1990) and previously used by Abalos (1997) to characterize omphacite fabrics.

In this study, the omphacite LPO were characterized by eigenvalues and eigenvectors from the distributions of three crystal directions **a*** (100), **b**[010] and **c**[001], which are mutually perpendicular in the monoclinic

crystal system, and typically show the strongest preferred orientations among the omphacite axes (Godard and Van Roermund, 1995). Eigenvectors for omphacite distributions are denoted by $o_{1[xyz]}, o_{2[xyz]}, o_{3[xyz]}$, where $[xyz]$ is one of the three vectors **a*** (100), **b**[010] or **c**[001].

For the rutile LPO, the distributions of **a**[100] and **c**[001] axes were characterized by their eigenvalues and by the eigenvectors $r_{1[001]}, r_{2[001]}, r_{3[001]}$ for the **c**[001] axis. Because of the fourfold crystal symmetry about the **c**[001] axis of rutile with $a = b$, eigenvalues and eigenvectors for all directions $[uv0]$ normal to **c**[001] are equal. Furthermore, eigenvectors for $[uv0]$ (like **a**[100]) and **c**[001] are related by $r_{1[uv0]} = r_{3[001]}$, $r_{2[uv0]} = r_{2[001]}, r_{3[uv0]} = r_{1[001]}$.

3.3. Shape fabrics

Shape preferred orientation (SPO) was deduced from the angles between the elongation of omphacite grains and the border of the thin section in the *XZ* and *XY* sections (*X* = lineation; *XY* = foliation plane). For each grain, the angle of the longest grain axis to the reference line was measured, irrespective of shape and size of the grains. From the list of measured angles, a mean elongation direction and an average aspect ratio were derived by a projection procedure similar to the SURFOR technique described by Panozzo (1983, 1984). The obtained mean elongation directions were subsequently used as refined references for lineation and foliation, and the aspect ratios as ratios *X/Y* and *X/Z* of the grain shape ellipsoid, respectively.

4. Omphacite fabrics

4.1. Crystallographic fabrics

The LPO of omphacite in 20 eclogite samples are presented in Fig. 8 as fabric diagrams of the **b**[010] and **c**[001] axes, as well as **a*** (100) and (110) poles, and as

Fig. 8. LPO of omphacite in pole figures (*left*) and inverse pole figures (*right*). All figures on lower hemisphere equal area projection, if applicable reduced by the inversion symmetry. Density in logarithmic scale in multiples of random distribution (mrd). In the pole figures, normal to foliation plane S is vertical, and lineation L is horizontal. A reference key is given with crystallographic directions for the inverse pole figures, where the *X* and *Z* figures show the frequency of crystal directions to align parallel to the lineation and the foliation normal, respectively. Field orientations of foliation and lineation for each sample are indicated below the sample number.

inverse pole figures of the foliation normal (*Z*) and of the lineation (*X*). Omphacite fabrics are typically divided into three principal categories ranging from pure S- to pure L- type fabrics:

4.1.1. S-type fabrics

In S-type fabrics (samples G70–G77, G81–G84, F70): where **b**[010] is maximum normal to foliation and **c**[001] is randomly distributed in the foliation plane (S). The poles of (100) are also randomly dispersed within S, and consequently the poles to (110) describe two small circles around the foliation normal at an angle of about 45°, which is the angle between (110) and **b**[010]. Deviations from the perfect S-type fabric can be recognized by maxima of **c**[001] close to the lineation (L), and by various concentrations of **a***(100) and (110) perpendicular to L. Two samples (G78 and G79) present a different S-type fabric, as the maxima along the **c**[001] girdle are nearly normal to L. Consequently, the girdle of **a***(100) has a maximum close to L, and two (110) maxima are at approximately ±45° from L away from S. This fabric type has so far only been reported in clinopyroxenes from rocks with minor clinopyroxene contents (Ji et al., 1993; Siegesmund et al., 1989), but never in

eclogites. A misidentification of the *X* and *Y* strain directions in the thin or SEM sections was first thought to be responsible for this observation, but the textures differ by more than just a rigid rotation of the reference frame. In both samples, the maximum of **b**[010] widens towards a girdle normal to L, which is in agreement with the girdle of **b**[010] observed in all the other samples, which display S- or LS-type fabrics. The S-type fabrics are generally sharp with a texture index between $J_{G77} = 4.26$ and $J_{G72} = 2.71$.

4.1.2. SL- and LS-type fabrics

SL- and LS-type fabrics are intermediate between S- and L-type (samples G80, G86, G100, H3), for which **b**[010] is distributed in a girdle normal to L and **c**[001] in a girdle parallel to the foliation plane. The girdle of **b**[010] contains a maximum normal to S, and the girdle of **c**[001] a maximum parallel to L. When the L-character is stronger developed than the S-component, **a***(100) and (110) are arranged on girdles normal to L, with a maximum of **a***(100) generally lying in S, and maxima of (110) more away from S. The texture strength is generally weaker in these samples than in those with an S-type fabric and ranges between $J_{G100} = 2.76$ and $J_{G80} = 1.88$.
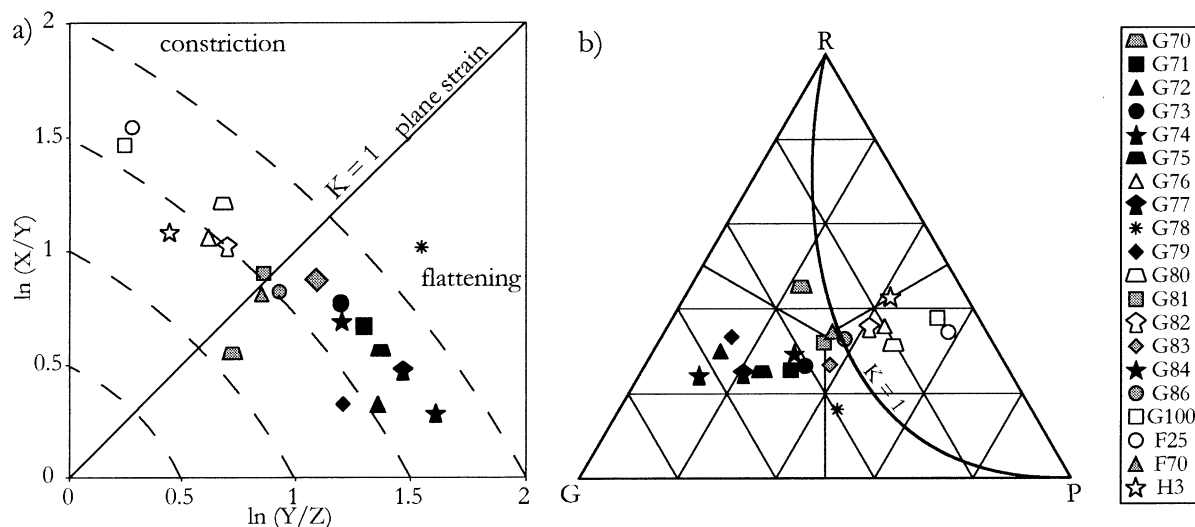

Fig. 9. Eigenvalues and eigenvectors of the omphacite **b**[010], **c**[001] and **a***(100) pole figures. (a) Eigenvalues plotted in triangular fabric diagrams based on the indices *point*, *girdle* and *random*. (b) Eigenvectors o_1 (circles), o_2 (squares), o_3 (triangles) on equal area lower hemisphere projection. Normal to foliation plane S is vertical, and lineation L is horizontal. Samples displaying S-type fabrics are presented by black symbols, and samples with LS-type fabrics by grey symbols.
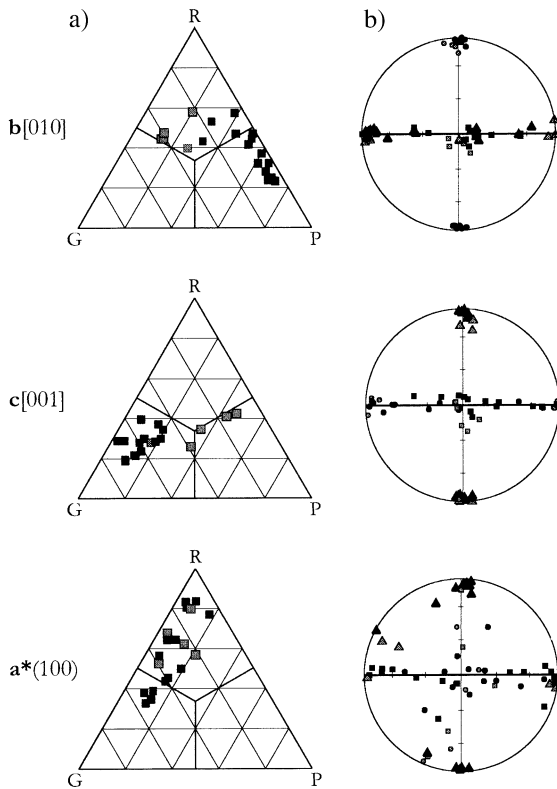
a)

b)

Fig. 10. LPO of rutile (*left*) and quartz (*right*) in pole figures on lower hemisphere equal area projection, if applicable reduces by the inversion symmetry. Density in logarithmic scale in multiples of random distribution (mrd). Normal to foliation plane *S* is vertical, and lineation *L* is horizontal.

4.1.3. L-type fabrics

In L-type fabrics, **c**[001] is parallel to lineation and **b**[010] is distributed within a girdle normal to L. This fabric type is rare in the Vendée eclogites and has been observed only in sample C22 (Fig. 13 in Godard and Van Roermund, 1995) and, to a lesser extent, in sample H3.

Characteristics of the fabric types are also visible in the inverse pole figures. For the S-type fabric, the

foliation normal (*Z*) aligns with **b**[010] and the lineation (*X*) lies in the plane normal to **b**[010], somewhat preferred close to **c**[001]. In the LS-type fabric, the foliation normal (*Z*) defines a girdle normal to **c**[001] which includes **b**[010], (110) and **a*** (100), whereas the lineation (*X*) aligns preferentially in a girdle normal to **b**[010] with a maximum parallel to **c**[001].

4.2. Correlation with the shape fabric

Shape-preferred orientations (SPO) of the studied eclogite samples (Fig. 9) range from strongly planar (samples G74, G72, G77, G78, G79) through intermediate to strongly linear (H3, G100, F25). At the scale of the quarry, no clear evolution is observed along the profile although omphacite crystals from samples originating from the NE side of the quarry seem to be more oblate (G80, G81, G82, G86).

A general correlation is observed between the types of shape and crystallographic fabric as the samples displaying a crystallographic S-type fabric are generally foliated, while the samples presenting a crystallographic LS-type fabric are lineated. There are few exemptions from this rule (G76, G82). No quantitative correlation could be obtained between the strengths of the shape fabrics and that of the LPO in contrast to the observation of Godard and Van Roermund (1995). The ranges in the strength of both the SPO and LPO are rather narrow for this data set, so that such correlation may not be noticeable. Some uncertainty also remains about the strength of the measured SPO because of the semi-quantitative approach applied (see Section 3.3). On the other hand, at the large strain involved in the deformation of the eclogite, it is not necessarily to be expected that the SPO would reflect the finite strain ellipsoid, and that the LPO would monotonously vary with finite strain neither. Indeed, high strain torsion experiments (e.g., Bystricky et al., 2000; Pieri et al., 2001) have shown that steady-state SPO and LPO develop through dynamic recrystallization in highly sheared rocks, and do not vary further with finite strain.

Fig. 11. Omphacite grain shape fabrics. (a) Logarithmic Flinn diagram with *X, Y, Z* representing the lengths of the principal axes of a mean grain shape ellipsoid. (b) Triangular fabric diagram based on the indices *point* (P), *girdle* (G) and *random* (R) as defined by Vollmer (1990). The indices were calculated from the shape ratios with $e_1/e_2 = X/Y \geq 1$, $e_2/e_3 = Y/Z \geq 1$, $e_1 + e_2 + e_3 = 1$ according to $P = e_1 - e_2$, $G = 2*(e_2 - e_3)$, $R = 3* e_3$. Elongated shapes correspond to the point field (open symbols), flattened shapes to the girdle field (black symbols), plane strain shapes in between (grey symbols).

(b)
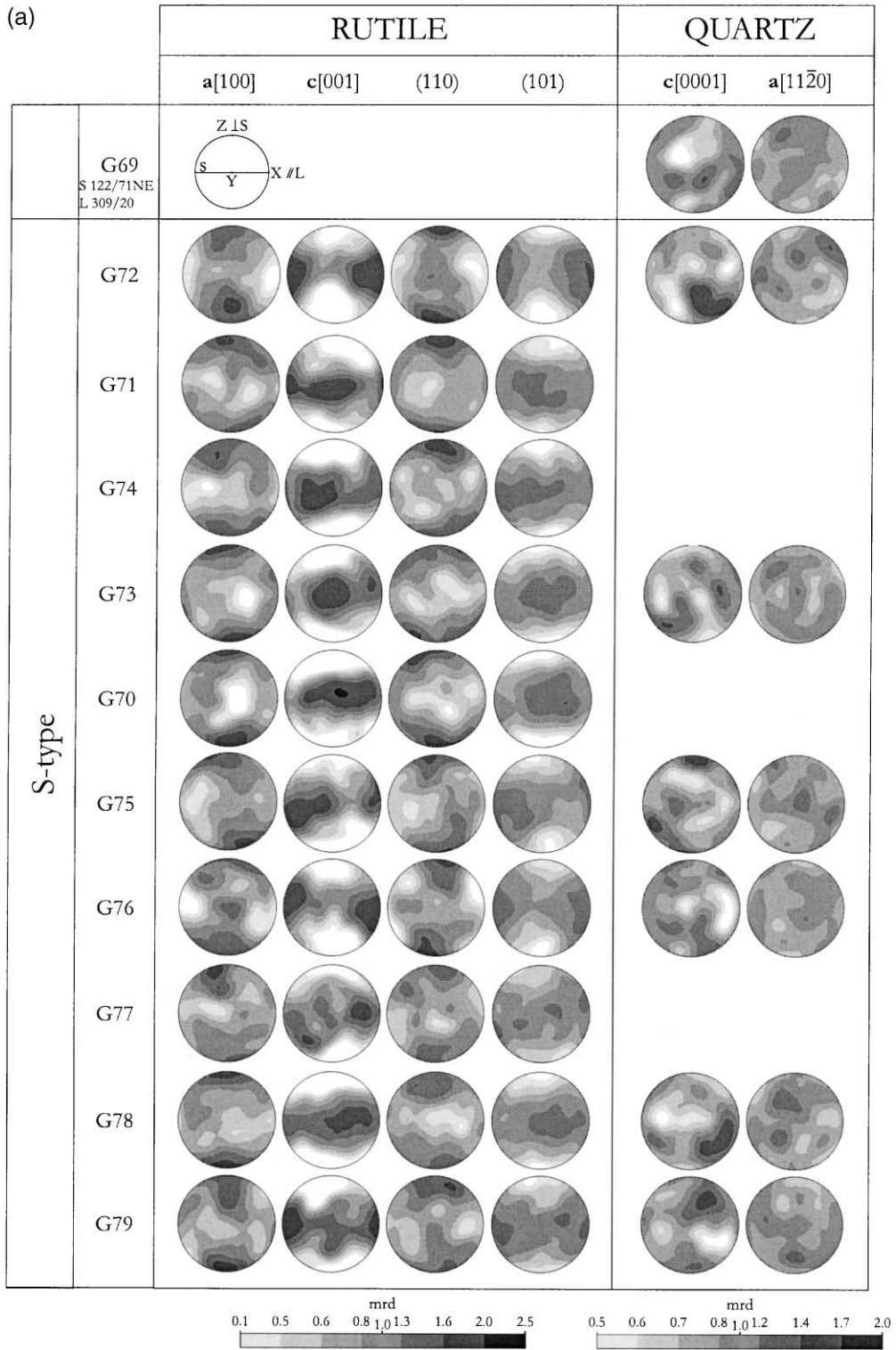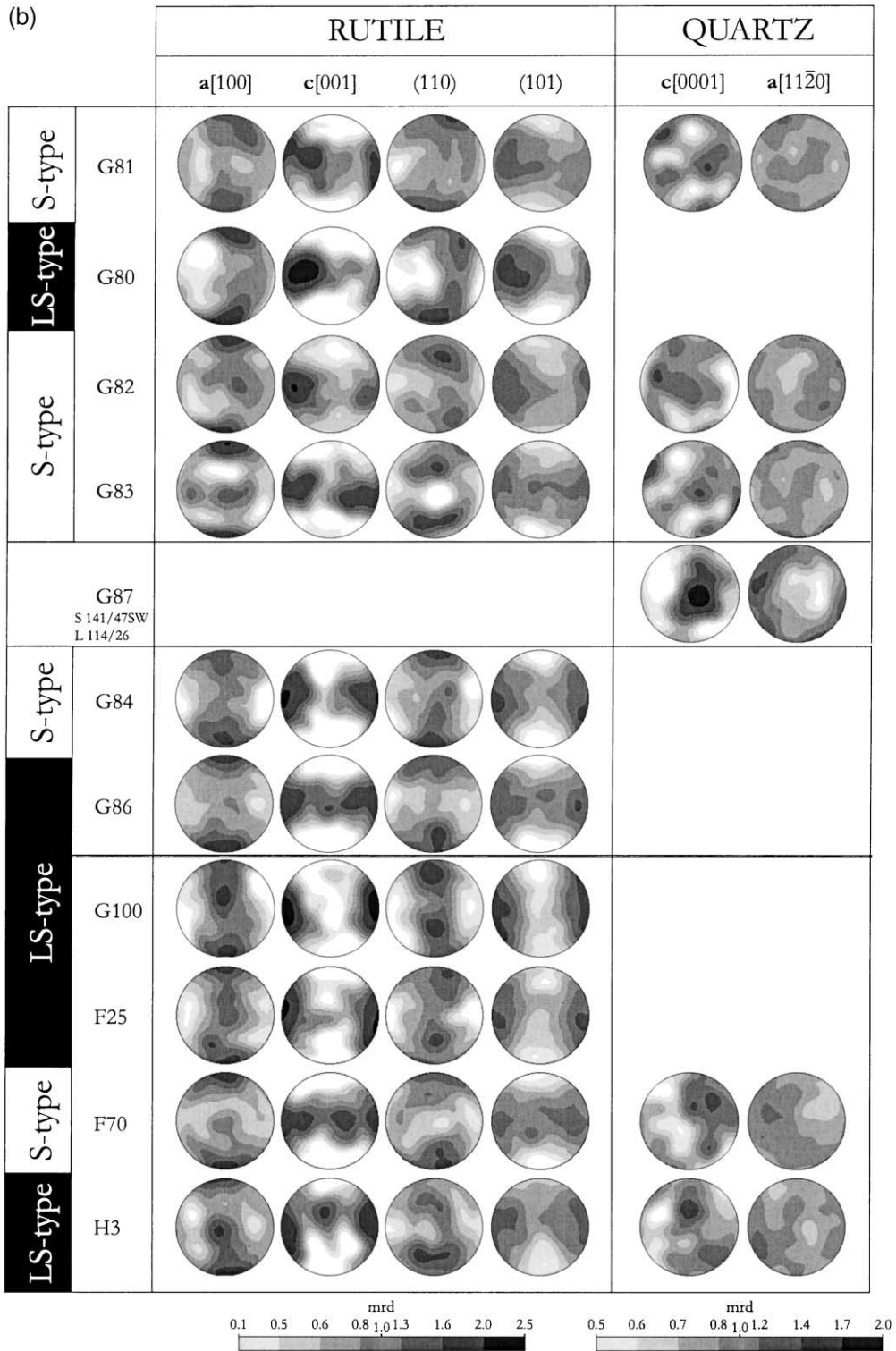
4.3. Eigenvalues and eigenvectors

Pole figures of **b**[010], **c**[001] and **a*** (100) of omphacite were characterized by eigenvalue distributions and eigenvector orientations as presented in Fig. 10. Based on the eigenvalues, the previous classification of the fabrics as S- and LS-type is reinforced. For the S-type fabrics, eigenvalues are characterized by a strong *point* component for the **b**[010] direction and a strong *girdle* component for the **c**[001] direction. In the LS-type fabrics, eigenvalues for **b**[010] still contain an important *point* component, while they would plot in the *girdle* field for true L-type fabrics. Similarly, the eigenvalues for **c**[001] would be in the *point* field for pure L-type fabrics, but still contain an important *girdle* component for the LS-type fabrics. Only three samples (H3, F25 and G100) with LS-type fabrics actually reach in the *point* field. The *random* contribution is lowest for **c**[001], suggesting that preferred orientation of **c**[001] fabric is strongest. Eigenvalues for **a*** (100) plot in the *random* field for the LS-type fabrics, while for the S-type fabrics they often preserve a substantial *girdle* component.

Plots of the eigenvectors of the **b**[010], **c**[001] and **a*** (100) distributions with respect to the structural reference frame show that the first eigenvector for **b**[010] plots generally close to the foliation normal. For LS fabrics, the first eigenvector for **c**[001] plots close to the lineation. For S-type fabrics, $o_{1[001]}$ and $o_{2[001]}$ are randomly spread in the foliation plane.

In a previous study, Abalos (1997) used misalignments between the eigenvectors and the structural reference frame to deduce a sense of shear of the deformation. More specifically, he analyzed the angles between $o_{1[010]}$ or $o_{3[001]}$ and the pole to the foliation. On our data set of 20 eclogite samples, the first angle (between the eigenvector o_1 for **b**[010] and the normal to the foliation within the *XZ* plane) reaches a maximum of 9°, and the average absolute angle for all the samples is 2.5°. Similarly, the obliquity between the eigenvector $o_{3[001]}$ and the foliation normal reaches a maximum angle of 7°, and the average absolute angle is less than 3°. Moreover, the sense of the obliquity with respect to lineation varies from clockwise (F25, F70, G71, G76, G77, G80, G82) to anticlockwise (G100, G70, G72 to G75, G78, G79, G81, G83, H3) without any obvious consistency. Therefore, the misalignments cancel each other out on average over all samples,

resulting in very small average total angles of 0.1° and 0.8°, respectively.

In summary, the LPO of this data set do not significantly deviate from orthorhombic symmetry aligned with the structural reference frame. Therefore, they did not record any non-coaxial (shear) deformation in the eclogites, which may well have occurred as indicated in the surrounding gneisses. Thus, we conclude that the obliquity between the omphacite LPO and the structural framework is not robust enough to be used for reliable shear sense determination.

5. Rutile fabrics

5.1. Crystallography of rutile

Rutile is the high temperature polymorph of TiO_2 and the most common form in nature. It belongs to the tetragonal crystal system ($a = b \neq c$, $\alpha = \beta = \gamma = 90°$) and to the highest symmetry point group in this system (4/mmm), implying that **a**[100] and **b**[010] are equivalent directions. The lattice is flattened with **c**/**a** ratio of 0.64, while the crystals grow elongated parallel to the **c**[001] axis, both similar to omphacite.

In compression experiments performed on stoichiometric single crystals of rutile, two glide systems have been activated above 875 K, most dominantly $\langle \bar{1}01 \rangle \{101\}$ and also $\langle 001 \rangle \{110\}$. Sets of experiments were run at temperatures between 800 and 1700 K, under oxygen partial pressure of 1 atm, at constant strain rates between 1.4×10^{-5} and 5.65×10^{-4} s^{-1}, for compression parallel to [001] and at 45° from [001] to a maximum strain of 1.26% (Blanchin and Fontaine, 1975; Blanchin and Faisant, 1979; Blanchin et al., 1990). Data on active slip systems in naturally deformed rutile or LPO of experimentally deformed polycrystalline rutile aggregates have not been reported yet. Twinning occurs on {101} planes.

5.2. LPO patterns of rutile

The LPO of rutile are consistent throughout the studied samples and can be arranged into two groups, as shown in Fig. 11. Although the fabrics are weakly developed, a tendency of the rutile fabric to duplicate the omphacite LPO is clearly visible. Therefore, the

terminology used for omphacite LPO classification is also followed for the rutile LPO without reference to the rutile grain shape.

5.2.1. SL-type fabrics

SL-type fabrics can be defined in samples G70, G71, G73 to G75, G77 to G79, G81, G83, G84 and F70, where maxima in **a**[100] and therefore **b**[010] are normal to foliation, while **c**[001] is dispersed in the foliation plane and often concentrates close to lineation. However, for some samples (G70, G73), the maximum in **c**[001] is off the lineation or even concentrates in a direction nearly normal to L, without correspondence to a similar behaviour in the omphacite fabrics.

5.2.2. LS-type fabrics

LS-type fabrics are recognized in samples G72, G76, G80, G82, G86, G100, F25 and H3. In this type of fabrics, the maximum of **c**[001] is close to lineation and **a**[100] and **b**[010] spread out in a great circle normal to the lineation.

Comparison of the LPO of omphacite and rutile for each sample shows a clear correlation. In the samples displaying an omphacite S-type fabric, the fabric of rutile is predominantly planar, while in the samples displaying an omphacite LS-type fabric, the fabric of

rutile is more linear. Only a few samples do not respect this correlation, where the omphacite fabric is an S-type while the rutile fabric resembles more an LS type (G72, G76, G82, G84).

5.3. Eigenvalues and eigenvectors

The pole figures of rutile were characterized by eigenvalues and eigenvectors analogously as for omphacite (Fig. 12). Both the eigenvalues for **c**[001] and **a**[100] plot mostly in the *random* field. Samples with an LS-type fabric sometimes contain a *point* contribution for **c**[001], which should be there for a perfect L-type. For the SL type, eigenvalues for **c**[001] have a stronger *girdle* component. Eigenvalues for **a**[100] are always close to *random* with only minor *girdle* tendency.

Plots of the eigenvectors for **c**[001] with respect to S and L show that $r_{3[001]}$ plots always close to the foliation normal. For LS-type fabrics, the eigenvectors $r_{1[001]}$ plot towards L, while for S-type fabrics, $r_{1[001]}$ and $r_{2[001]}$ are spread randomly within S. Any fabric obliquity would be deduced from the angle between $r_{3[001]}$ and the pole to S. The absolute average obliquity (azimuth angle in the *XZ* plane) for all the studied samples is 1.3°, and 0.8° for the samples in the quarry. Therefore, the rutile LPO does not reflect any representative shear component.
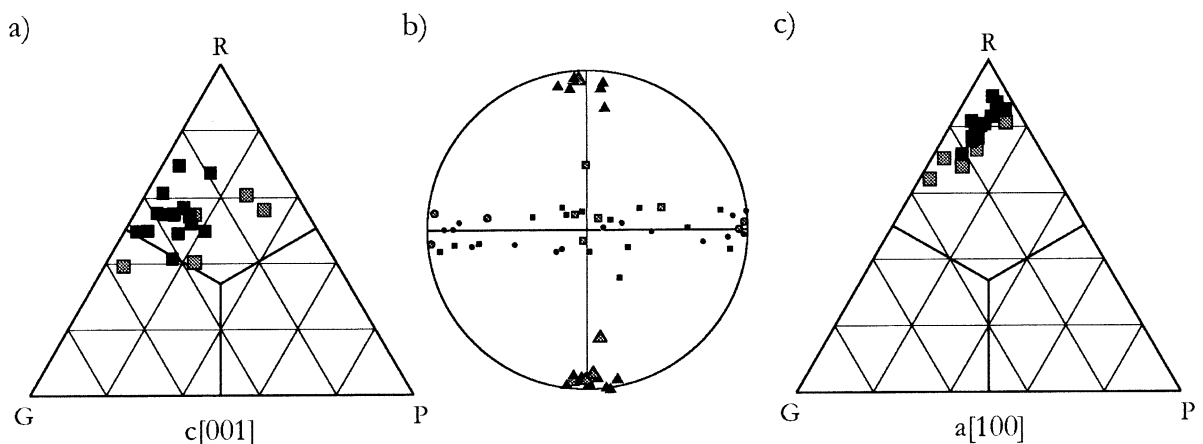
Fig. 12. Eigenvalues and eigenvectors of the rutile pole figures for 20 eclogites samples (see Fig. 11). (a) Eigenvalues for **c**[001] plotted in a triangular fabric diagram. (b) Eigenvectors r_1 (circles), r_2 (squares), r_3 (triangles) for **c**[001] on equal area lower hemisphere projection. Normal to foliation plane S is vertical, and lineation L is horizontal. The eigenvectors for **a**[100] are parallel to those of **c**[001] in reverse order (3 to 1). (c) Eigenvalues for **a**[100] plotted in a triangular fabric diagram. Symbol color according to the omphacite fabrics of the same samples (see Fig. 10).

5.4. Comparison of eigenvectors for omphacite and rutile

As shown above, the absolute orientation ellipsoids of omphacite and rutile are parallel to the structural reference frame within the error limits to define the reference frames themselves. This error is eliminated when comparing the orientation of omphacite and rutile LPO relative to each other.

For each sample, the position of the eigenvectors for rutile relative to the ones for omphacite was compared, that is the angles between $r_{1[010]}$ (which is equal to $r_{3[001]}$) and $o_{1[010]}$, and between $r_{3[001]}$ and $o_{3[001]}$ (Fig. 13). Although the absolute average asymmetry is less than 2.5° in both cases, subgroups can be formed where the obliquity is higher. In the SW side of the quarry (samples G70–G79), the obliquity is consistent within the samples (except of sample G71). On average, $r_{3[001]}$ is displaced from $o_{1[010]}$ (respectively $o_{3[001]}$) by an anticlockwise rotation of 6° around the structural Y-axis. In the northern side of the quarry (samples G81–G84), $r_{3[001]}$ is deduced by a clockwise rotation around Y of 5.5° from $o_{1[010]}$ and of 4.5° from $o_{3[001]}$ on average. The transition between clockwise and anticlockwise rotation occurs at sample G80, where a change in lineation plunge occurs. The obliquity in the lineated samples is generally much weaker (1–2°) than in the foliated samples.

The observed asymmetry might be used for shear sense determination. From previous work also in the surrounding gneisses, the general sense of shear in the quarry area is believed to be dextral, so that in the SW part of the quarry, the rutile LPO rotated against the sense of shear relative to the omphacite fabric.

Fig. 13. Comparison of the eigenvectors $o_{1[010]}$, $o_{2[010]}$, $o_{3[010]}$ (black dot, square and triangle, respectively) and $o_{1[001]}$, $o_{2[001]}$, $o_{3[001]}$ (grey circle, square and triangle) of omphacite and $r_{1[001]}$, $r_{2[001]}$, $r_{3[001]}$ (white circle, square and triangle) of rutile for 20 eclogites samples; equal area lower hemisphere projection. Normal to foliation plane S is vertical, and lineation L is horizontal. Most of the eigenvectors are nearly parallel to the structural reference frame defined by S and L without any systematic deviations. The angles between $o_{1[010]}$ and $r_{1[001]}$ (=$r_{3[001]}$) (black dot and white triangle), or between $o_{3[001]}$ and $r_{3[001]}$ (grey triangle and white triangle), which are all nearly normal to the foliation, might be used to infer a sense of shear with respect to the flow plane and the flow direction. The arrow pairs indicate the sense of rotation of the rutile fabric with respect to the omphacite fabric.
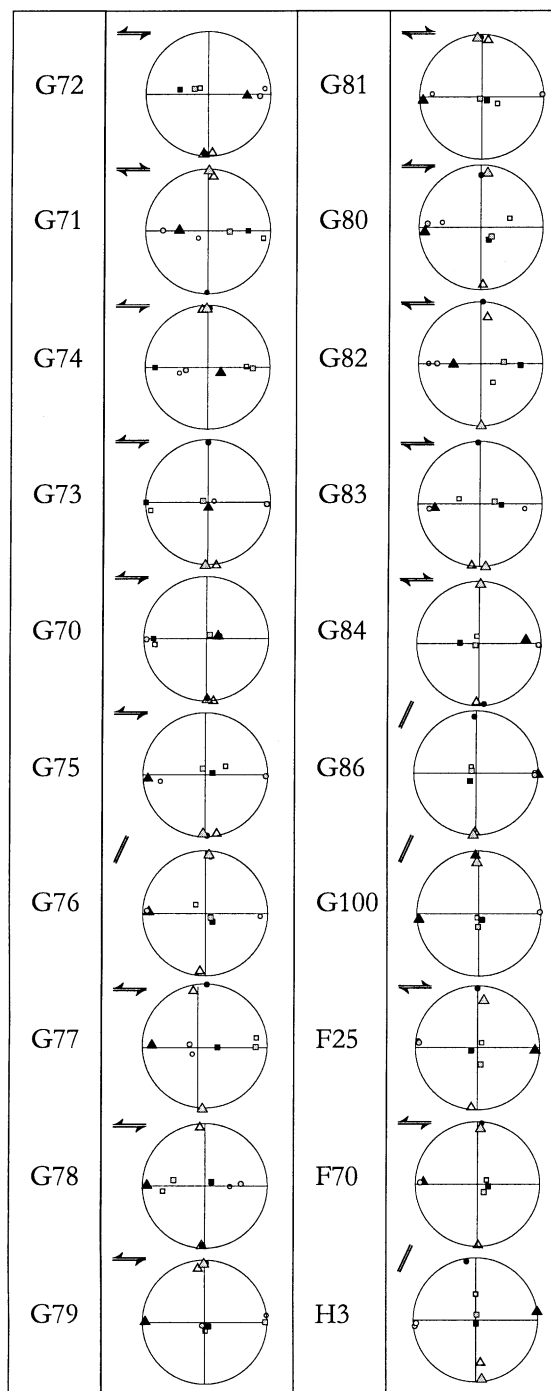
6. LPO of quartz

6.1. LPO of quartz in the eclogites

Fabrics of quartz in the eclogite are presented in Fig. 11. None of the pole figures show consistency throughout the studied samples. The **c**[0001] axis pole figures present patterns varying from single point maxima (G72, G78, G79 and G82) to more complex patterns with multiple point maxima (G73, G75, G76, G81, G83 and H3). Consequently, pole figures of **a**[11$\bar{2}$0] also differ for each sample. The strength of the textures is very low ($J_{G76} = 1.11$ to $J_{G82} = 1.26$) in all the samples indicating a texture close to random. Because of the difficulty to interpret the fabrics and of a rather poor confidence in their significance, no sense of shear is deduced from the quartz LPO in the eclogite samples.

6.2. LPO of quartz in the gneisses

The fabric of quartz in the gneiss sample G69, describes also a complex pattern, and because of the low texture index ($J_{G69} = 1.20$), the fabric is interpreted as random. The LPO of sample G87 is characterized by an elongated point maximum of **c**-axes nearly parallel to *Y*. The **a**[11$\bar{2}$0] axes define a girdle spread out at the periphery of the pole figure normal to the maximum of **c**[0001] with a point maximum near the lineation, rotated clockwise by about 15°. The texture strength in this sample is highest ($J_{G87} = 1.35$) of all quartz data and can be interpreted as produced by simple shear at medium-grade metamorphic conditions where prism $\langle$**a**$\rangle$ slip is dominant, producing the **c**[0001] maximum near the *Y*-axis (according to Schmid and Casey, 1986). The asymmetry with respect to *X* and *Z* in the **c**- and **a**-pole figures of sample G87 indicates a dextral sense of shear, in agreement with the dextral strike slip movement in this area.

7. Local LPO variations in omphacite

7.1. Sample description and technique

Local LPO measurements were performed in polycrystalline omphacite included within a single hollow garnet (Fig. 14a) in sample C22 of Godard (1988) and Godard and Van Roermund (1995). Two main domains of omphacite crystals were distinguished inside this garnet. In part C, omphacite crystals were presumably sheltered from any deviatoric stresses by the garnet crystal. Omphacite is fine-grained, slightly elongated and only weakly aligned. Very fine quartz and rutile grains occur. In part F, the garnet is broken and the omphacite deformed. Omphacite is coarser grained and the grains are even larger than in the matrix (part D). Omphacite crystals are strongly elongated with shape ratios up to 6:1. According to Godard (1988) and Godard and Van Roermund (1995), the omphacite inside garnet represents an early stage in the eclogite evolution, and escaped subsequent syn-eclogite-facies deformation due to the rigidity of garnet.

For a representative set of grains, the lattice and shape orientations were measured (for details see Table 1). The average direction of the long axis of all the grains measured represents the local apparent traces of foliation and lineation within the section plane. Best-fit axes for the crystallographic directions **b**[010] and **c**[001] were obtained from eigenvector calculations.

7.2. Results

The omphacite LPO (Fig. 14a) in part C is not random but presents a girdle of **c**[001] with a point maximum in the section plane. The **b**[010] and (110) pole figures display point maxima of similar intensity sub-perpendicular to the point maximum of **c**[001], and close to the eigenvector $o_{3[001]}$.

Fig. 14. Microstructures and LPO of omphacite enclosed in a skeletal hollow garnet that has been broken during deformation (sample C22 from Godard, 1988, and Godard and Van Roermund, 1995). (a) Polarized light micrographs, overview with red frames marking the enlargements. Broken garnet (A), garnet fragment (B), omphacite (C,D,F) and quartz (E). Pole figures of omphacite in the matrix (D), in the deformed omphacite (F1 and F2) and in the core of the garnet (C), density in logarithmic scale (mrd) on lower hemisphere equal area projection. The black dots represent the direction of maximum grain elongation within the section plane (trace of foliation). Eigenvectors o_1 (white dots), o_2 (white squares), o_3 (white triangles) are represented in the **c**[001] and **b**[010] pole figures. (b) Eigenvalues for **b**[010] and **c**[001] plotted in a triangular fabric diagram for the four parts defined above.
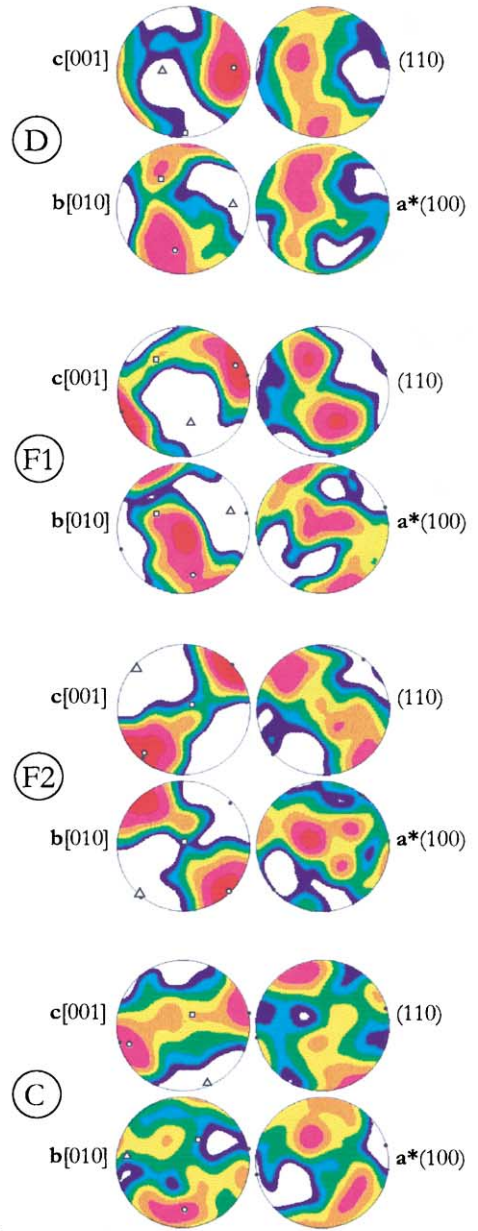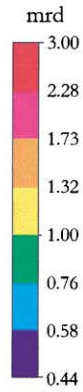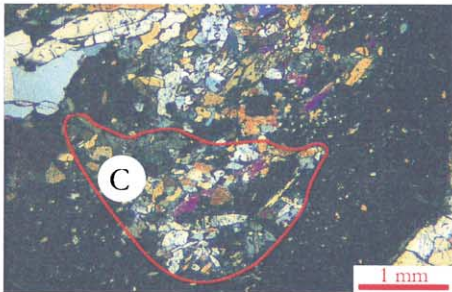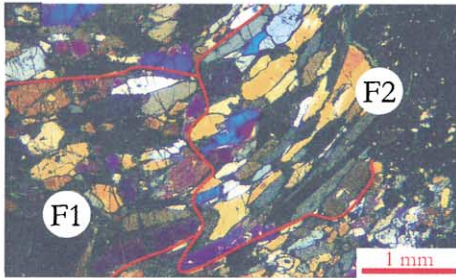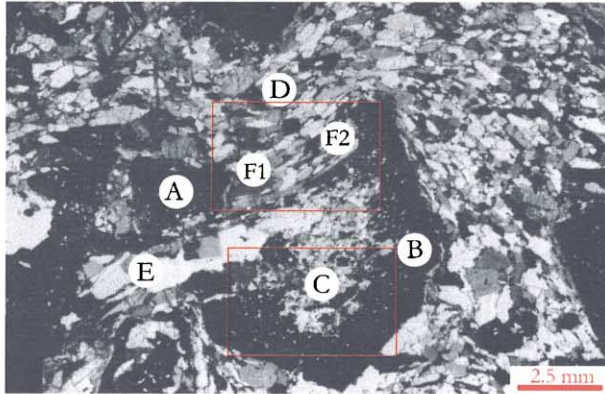
Table 1
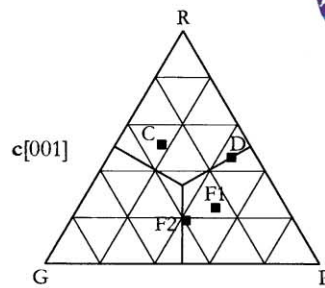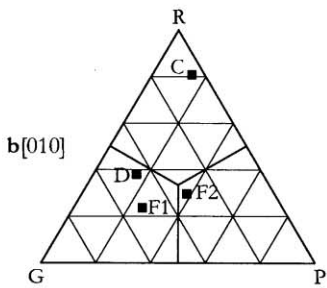Parameters of the LPO measurements in the studied eclogite samples. Sampling grid definition for omphacite (size of the grid, step size, total number of measurements, number of valid omphacite orientations). Number of manually measured rutile and quartz orientations. Texture indices for LPO of omphacite, rutile and quartz, based on Gaussian convolution of the individual orientation data using a smoothing width of 30°

Sample	G70	G71	G72	G73	G74	G75	G76	G77
OIM grid (mm)	20 × 8	18 × 8	18 × 9	24 × 8	19 × 10	19 × 9	20 × 9	22 × 6
@ step size (μm)	@ 200	@ 200	@ 200	@ 200	@ 200	@ 200	@ 200	@ 200
# total orientations	4141	3731	4186	4961	4896	4416	4646	3441
# omphacite orientations	1412	956	1271	993	1277	1284	618	891
Omphacite texture index J	4.1	4.1	2.7	4.0	2.9	2.2	3.0	4.3
# rutile orientations	170	180	190	180	180	200	160	150
Rutile texture index J	1.4	1.3	1.4	1.4	1.3	1.3	1.4	1.2
# quartz orientations	–	–	260	260	–	–	280	–
Quartz texture index J	–	–	1.2	1.1	–	–	1.1	–

Sample	G78	G79	G80	G81	G82	G83	G84	G86
OIM grid (mm)	16 × 10	19 × 8	22 × 6	14 × 8	20 × 9	16 × 9	13 × 12	11 × 6
@ step size (μm)	@ 200	@ 200	@ 200	@ 200	@ 200	@ 200	@ 200	@ 200
# total orientations	4131	4186	3441	2911	4646	3726	4026	1705
# omphacite orientations	1067	1181	1308	1017	560	839	1370	605
Omphacite texture index J	3.3	3.4	1.9	3.6	2.9	3.4	2.2	2.5
# rutile orientations	180	170	200	180	180	80	170	160
Rutile texture index J	1.3	1.3	1.7	1.3	1.3	1.5	1.5	1.4
# quartz orientations	290	300	–	170	260	185	–	–
Quartz texture index J	1.1	1.2	–	1.2	1.3	1.2	–	–

Sample	F25	F70	G100	H3	C22 (D)	C22 (F1)	C22 (F2)	C22 (C)
OIM grid (mm)	20 × 6	18 × 4	20 × 7	18 × 8	–	–	–	–
@ step size (μm)	@ 200	@ 200	@ 200	@ 200	manual	manual	manual	manual
# total orientations	3131	2911	3636	3731	–	–	–	–
# omphacite orientations	931	581	488	630	107	33	83	117
Omphacite texture index J	3.3	2.5	2.8	2.8	4.0	4.8	4.1	2.1
# rutile orientations	160	170	160	170	–	–	–	–
Rutile texture index J	1.4	1.4	1.7	1.3	–	–	–	–
# quartz orientations	–	250	–	150	–	–	–	–
Quartz texture index J	–	1.2	–	1.2	–	–	–	–

In part F, omphacite was separated into two fractions that have different SPO. For both parts, the omphacite pole figures display LS-type fabrics with a girdle of c[001] normal to a girdle of b[010], and both girdles contain point maxima perpendicular to each other. On the left-hand side (F1), the girdle of c[001] axes is sub-horizontal, and the girdle of b[010] sub-vertical suggesting that S is close to the section plane. In the right-hand part (F2), both girdles of c[001] and b[010] intersect in the center, suggesting that S is nearly vertical. In the two parts, the eigenvector $o_{1[001]}$ is subparallel to the average elongation of the measured omphacite grains. As there was only one section plane available, no three-dimensional shape analysis could be performed to determine the position of the actual foliation plane.

In the matrix (D), the maxima of c[001] and b[010] are wider because orientations were sampled in zones where the omphacite flows around the garnet. As in the other parts, the LPO has a maximum of c[001] sub-parallel to the average grain elongation and a girdle of b[010] perpendicular to it. Although perturbed by the presence of the garnet, this fabric corresponds to a weak L-type fabric. This LPO is similar to the one obtained by Godard and Van Roermund (1995) on a sample from the same locality.

The texture index has increased from $J = 2.1$ (part C) to $J = 4.1$ (F1) and $J = 4.8$ (F2), respectively. The

LPO eigenvalue analysis (Fig. 14b) shows distributions in the random field for part C, compared to intermediate distributions between *point* and *girdle* in F1 and F2. Keeping in mind that the counting statistics were limited due to the finite number of grains measured, we interpret the omphacite LPO in domains F1, F2 and D to be of similar type, with **b**[010] eigenvalues in the *girdle* field and **c**[001] eigenvalues towards the *point* domain. They are oriented with respect to their local structural reference frames, which are rotated relative to each other. The LPO in part C is distinct from that in the other three domains.

We conclude that in the vicinity of the garnet, the strain intensity increased from part C to parts F and D. The LPO evolved from a weak S-type in part C to strong SL- and LS-types in parts F and D due to a change in deformation regime of omphacite from inside to outside of the garnet. As the strain ellipsoid rotated around the garnet, the orientations of the LPO maxima rotate accordingly between parts F and D without modifying the principal LPO type.

8. Discussion

8.1. Deformation mechanisms

8.1.1. Omphacite deformation mechanisms

The omphacite S-type and L-type LPO are typical fabrics for clinopyroxene in high-pressure rocks. These fabrics have been reported by numerous authors (Avé Lallemant, 1967; Binns, 1967; Kumazawa et al., 1971; Baker and Carter, 1972; Carter et al., 1972; Engels, 1972; Helmstaedt et al., 1972; Boudier, 1978; Godard, 1981; Van Roermund and Boland, 1983; Kuijper et al., 1985; Godard, 1988; Van Roermund, 1992; Boundy et al., 1992; Barruol and Mainprice, 1993; Godard and Van Roermund, 1995; Abalos, 1997; Brenker, 1998). Its origin still remains under discussion. In a previous study, Godard and Van Roermund (1995) examined the possibility to develop this fabric by glide on a single slip system, as well as on multiple slip systems. They concluded that the fabric with (010) parallel to S cannot be exclusively produced by dislocation creep because there has no [$u0w$] (010) slip system been reported for omphacite. Therefore, other mechanisms, such as diffusion creep with concomitant anisotropic growth

and dissolution, should be involved, as already suggested by Helmstaedt et al. (1972) using the terms of crystallization under non-hydrostatic stress. The hypothesis of directed growth is further based on the work of Van Panhuis-Sigler and Hartman (1981), who showed that the attachment energies in clinopyroxenes are minimum for the plane (010), intermediate for (100) and maximum for (001), and so are the face growth and dissolution rates. Similarly, the elastic modulus C_{22} associated to the **a***(100) direction is lower than elastic modulus C_{11} (associated to **b**[010]), and both are lower than C_{33} (associated to **c**[001]) in a similar trend for all clinopyroxene minerals (Bass, 1995). Consequently, the compressibility is lower in the **c**[001] direction than normal to it. Moreover, in clinopyroxenes, diffusion rates are about one order of magnitude higher in the direction parallel to **c**[001] than normal to **c**[001]. For all these reasons, those crystals that grow fastest have **c**[001] parallel to the tension direction (lineation) and **b**[010] parallel to the compression direction (foliation normal). Vice versa, those with **b**[010] parallel to the tension direction and **c**[001] parallel to the compression direction dissolve fastest (Fig. 15). These processes favor crystals oriented with (010) parallel to S, and [001] parallel to L. The LPO of undeformed omphacite veins, with **c**[001] normal to the vein walls, i.e. parallel to the tensional (growth) direction (Philippot and Van Roermund, 1992), can hardly be explained in any other way. Overgrowths of omphacite resulting from garnet translations parallel to the tension direction also strongly support this hypothesis (Fig. 3b in Godard and Van Roermund, 1995).

Further conclusions can be obtained from the examination of the omphacite fabric inside and outside of the broken garnet of Section 7. Outside of the U-shaped garnet, omphacite behaved plastically as it wrapped around the garnet and was subjected to high stress and strain gradients. The omphacite LPO varies with the SPO, so that the principal axes of lattice and grain shape preferred orientations remain approximately in the same orientation relative to each other. This shows that both the shape and crystallographic fabrics follow the stress trajectories in the inhomogeneous stress field around the stiff garnet. Omphacite inside the garnet was presumably sheltered from those deviatoric stresses. Furthermore, crystal growth
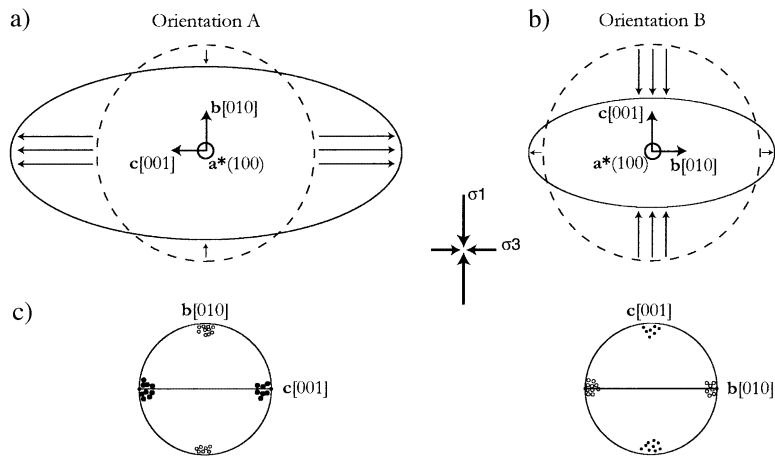
Fig. 15. Schematic illustration of the effect of anisotropic dissolution and precipitation rates on the omphacite LPO. (a) Grain A oriented with **c**[001] parallel to σ_3 grows rapidly parallel to **c**[001] and dissolves slowly parallel to σ_1. (b) Grain B oriented with **b**[010] parallel to σ_3 grows slowly parallel to **b**[010] and dissolves rapidly parallel to σ_1. (c) The process favours grains in the orientation *A*, while grains in orientation *B* ultimately vanish, thus producing the [001] (010) fabric.

occurred concomitantly with deformation, as proved by the variation in grain size between the weakly deformed zone C and the highly deformed zones F and D (Fig. 14). Two main growth processes can occur during deformation. Strain-induced grain boundary migration can hardly have produced the observed SPO and LPO, whereas oriented growth in a deviatoric stress field could account for the observed facts (see discussion in Godard and Van Roermund, 1995, pp. 1439–1440). Moreover, the omphacite grains in parts F and D do not show any deformation features, such as mechanical twins, undulous extinction or subgrains, and such features do not develop during oriented growth. The fine-grained omphacite in part C (inside the garnet) can be regarded as protected from the deviatoric stress field and as not largely subjected to anisotropic growth processes. Its LPO, which is weak but not random, could either be inherited from the fabric of the pre-eclogite rock or result from an early stage of plastic deformation prior to the garnet growth. The maximum of (110) poles suggests that the [001]{110} slip system could have been active during this stage.

We conclude that diffusion creep with oriented growth is likely a main deformation mechanism in omphacite and that it contributes to its LPO development. The geometry of the shape and crystallographic

fabrics might therefore also be representative of the stress regime (direction and magnitude ratios of principal stresses). However, because of the anisotropy of omphacite, dislocation and diffusion creeps could operate in distinct grains, depending on the orientation of the latter in the stress field.

8.1.2. Rutile deformation mechanisms

It is difficult to interpret the deformation mechanisms of rutile because of the lack of knowledge concerning the mechanical behaviour of this mineral. The LPO of rutile could be, for some part, the result of dislocation glide on [001](110), as suggested by the maximum of **c**[001] close to L and the maximum of (110) parallel to S in different samples (G72, G75, G76, G79, G81, G83, G84, G86, F70). This slip system has been observed to be active during compression experiments on single crystals. On the other hand, the rutile grain size is correlated with the omphacite grain size, which strongly suggests a similar deformation mechanism being active in both minerals. For example, rutile grains of the slightly deformed zone of sample C22 (zone C in Fig. 14) are numerous and very small, whereas grains are scarcer, coarser and more elongated in the strongly deformed zones of the same sample (zones F and D). Grain boundary migration cannot

explain the difference in size of the rutile grains between the strongly and slightly deformed zones, most of these grains are isolated from each other. On the other hand, diffusion creep with concomitant anisotropic growth/dissolution could well explain the **c**[001] preferred orientation parallel to the tensional direction, since rutile obviously grows faster parallel in this direction as proved by the needle-shaped habit of freely grown rutile crystals. Finally, mechanical twins are rather numerous in deformed rutile grains, and twinning has certainly also some importance here.

8.1.3. Quartz deformation mechanisms

As the strength of quartz is generally inferred to be lower than that of other eclogite mineral phases (clinopyroxene, garnet), it would be expected to carry a larger part of the bulk deformation, and consequently develop highly strained microstructures and deformation LPO. However, there is hardly any evidence of strong intracrystalline deformation and LPO development in quartz, as already observed by Binns (1967). Late static recrystallization and recovery can account for the lack of internal deformation features, for the straight grain boundaries, for the large grain size, and may have weakened any pre-existing LPO.

8.1.4. Summary of deformation mechanisms

Microstructures and LPO obtained from this study are indicative for the following deformation mechanisms:

- Despite of microstructural evidence for some intracrystalline deformation, omphacite is interpreted to have deformed mainly by diffusion creep. Deformation was carried by anisotropic growth and dissolution, which resulted in a clear LPO that varies from S to LS-type fabrics in correlation with the grain shape fabric.
- Rutile is discussed to have deformed under similar conditions and mechanisms as omphacite producing a LPO that is similar but weaker than the one developed in omphacite.
- Quartz shows neither evidence of strong intracrystalline deformation nor any strong LPO, presumably being recrystallized during retrogression.

8.2. Transition from S- to L-type fabrics

The transition between S- and L-type fabrics has been observed and interpreted for the first time by Helmstaedt et al. (1972) as being linked to the shape fabric of the grains (flattened and elongated, respectively) and due to a change in deformation regimes from compression to constriction. This interpretation has been widely accepted and also holds for the samples examined in this study. However, it has been recently put into question (Brenker, 1998; Brenker et al., 1999). According to these authors, the LPO of omphacite was not controlled by the deformation regime (i.e., strain geometry) but by a temperature-dependent change in Burgers vectors related to an ordering of cations. The ordering transition was determined from the omphacite composition using the equilibrium phase diagram for the system jadeite–aegyrine–augite (Carpenter, 1980). The authors suggested a transition from S-type to L-type omphacite fabrics when the temperature during deformation falls below 750°C, which is the critical temperature of ordering (space group transformation from $C2/c$ to $P2/n$) in omphacite. This transformation produces a split of the complete $1/2\langle110\rangle$ Burgers vector into two partial dislocations separated by a stacking fault at lower temperature. This increases the necessary energy for dislocation movement and thus the strength of the material. Using transmission electron microscopy, the authors observed such partial dislocations only in L-type eclogites, but did not find them in any of the investigated S-type eclogites. They also argued, that intracrystalline deformation features like subgrains should be visible preferentially in the stronger low temperature (L-type) eclogites, as they observed using orientation contrast image techniques in the SEM.

The results that we have obtained contain several points that do not support the latter hypothesis of LPO development. A new argument arises from the measured LPO of rutile, which are similar although weaker than the ones developed in omphacite. Where omphacite shows S-type fabrics, rutile has S-type or SL-type fabrics as well, and the same holds true with L-type fabrics. If the S–L transition would be the result of a switch in intracrystalline deformation mechanisms in omphacite, there is no reason why rutile should be affected and develop similar S- and L-type fabrics

under exactly the same external conditions. On the contrary, similarity of the fabrics in the two minerals suggests that they have undergone the same deformation events and strain history under flattening or constrictional strain. Another argument is that the samples from the quarry were taken at distances of a few meters, where the omphacite composition, temperatures during deformation and thus presumably the degree of order (Carpenter and Smith, 1981; Rossi, 1988) were homogeneous, while the fabrics vary. For instance, although G80 and G81 were taken along the profile within 3 meters, G81 displays a well-developed S-type fabric, while G80 has an LS-type fabric. More generally, all intermediate fabrics exist between the two extremes of S-type and L-type, most likely to be correlated to a continuous change in deformation conditions rather than to an abrupt space group transition. Finally, Godard and Van Roermund (1995) observed antiphase domains in all their samples, indicating that they all evolved through the space group transition from $C2/c$ to $P2/n$, whatever the fabric type.

8.3. Shear sense indications in eclogites

From the results obtained in this study, the omphacite LPO cannot be used for shear sense indication in the Vendée eclogites. The absolute obliquity between the fabric eigenvectors and the structural framework is less than 2.5°, which is well in the range of uncertainty that can be estimated by summing up the uncertainties from foliation and lineation determination and EBSD measurements. Similar arguments can be invoked for the obliquity of the rutile fabric (absolute obliquity 1.3°). This conclusion contradicts the results from Abalos (1997) who observed an asymmetry of 6–8° between the omphacite LPO and the foliation and lineation in eclogites from Cabo Ortegal (NW Spain). However, as the samples have a different origin there might be a stronger shear component in eclogites from the Cabo Ortegal than in the ones from Vendée.

The relative obliquity of the rutile LPO with respect to those of omphacite seems to be more consistent with angles around 5–6°. These angles are small and one can argue whether they are significant. However, considering the obliquity of two fabrics relative to each other in the same sample avoids many of the above uncertainties. In particular,

the relative rotation (i.e., misorientation) between the two sets of eigenvectors is independent from the absolute positions of the external reference frame and thus from the definition of S and L. Because the amount and sense of asymmetry show some consistency throughout the set of studied samples, we believe that the asymmetry is reproducible.

Bouchez et al. (1983) stated that one of the necessary conditions to use the asymmetry method is that the mineral phase being used for shear sense determination must be dominant in volume to eliminate flow heterogeneities. We are aware that rutile is not dominant in eclogites, thus the question arises whether the obliquity should be used for shear sense determination. In the particular case of rutile, little is known about the processes leading to LPO development (slip systems, relative critical shear stress, effect of temperature, strain rate) and therefore it is difficult to model and give more conclusive results about rutile as a shear sense indicator. Nevertheless, rutile orientations were collected manually over sampling areas similar in size to those of the OIM sampling grids to measure omphacite orientations. Potential flow heterogeneities have thus affected the fabrics of both minerals, and have been averaged in the omphacite and rutile LPO to a similar amount.

8.4. Rheology

From the results obtained in this study, it appears that anisotropic grain growth and dissolution are main transport processes in deforming eclogites at large depth. It may result either from the diffusion of point defects through the lattice (Nabarro–Herring creep), either from the diffusion of ions and molecules along grain boundaries (Coble creep) or from the migration of dissolved material along the grain and phase boundaries in the presence of a fluid phase (dissolution/precipitation creep). Either way, diffusion creep seems to play an important role in the deformation processes active in the lithosphere, and dislocation creep processes must not always predominate over the others, which is commonly assumed because of the high temperature and/or high stresses involved.

In a previous discussion, Godard and Van Roermund (1995, p. 1438) argued from the extrapolated creep laws for diopside that at low temperature unreasonable high stresses or low strain rates have to be considered to

accommodate strain in clinopyroxenes by dislocation creep, and that other deformation mechanisms may compete with it. This has been supported lately by experimental results of Bystricky (1998) and Bystricky and Mackwell (2001) who investigated the mechanical behaviour of hot-pressed diopside aggregates during stepping tests in compression experiments. The flow data obtained experimentally were satisfactorily fitted using Arrhenius laws. At high compressive stresses and high strain rates, the stress exponent n was close to 5, while towards low stresses and low strain rates, the stress exponent was $n \approx 1$, indicating a switch in deformation mechanisms from dislocation to diffusion creep towards low stresses and low strain rates. Although the conditions of deformation in the Earth are well different from the ones attained in such experiments, these results favor the hypothesis of deformation by diffusion processes. It is generally accepted that diffusion creep is grain size sensitive, as with increasing grain size the flux decreases, because the length of the diffusion path increases, respectively the number of potential sites for dissolution and precipitation per unit volume decreases. Diffusion creep is therefore expected to be negligible for large grain sizes, though the actual grain size sensitivity varies for different mechanisms involved. In the case of omphacite in the Vendée eclogites, despite a grain size that can reach several millimetres, evidence of deformation by diffusion creep processes has been observed, suggesting that in the Earth, the domain of geological conditions in which diffusion processes are active is wider than generally expected. If this is confirmed, Newtonian flow behaviour should be assigned to eclogites in models of exhumation processes.

9. Summary and conclusions

1. In the investigated eclogites from Vendée, the omphacite LPO range from S-type to L-type fabrics, and are correlated with planar and linear strain ellipsoids, respectively. S- and SL-types are dominant. These fabrics are interpreted as mainly due to diffusion creep with anisotropic growth/dissolution under a differential stress.

2. In Vendée, no significant asymmetry was observed between the omphacite LPO and the structural framework.

3. The LPO of rutile matches the LPO of omphacite and a similar distinction between S-type and L-type can be used as for omphacite. Rutile deformation mechanisms probably involved some dislocation creep as well as diffusion creep. Mechanical twinning also operated.

4. No significant asymmetry is observed between the rutile LPO and the structural framework.

5. A consistent asymmetry of the rutile LPO relative to the omphacite LPO is distinguished throughout the samples, that could potentially be used as a shear sense indicator in eclogites.

6. The weak quartz LPO and the absence of deformation features in the quartz grains is interpreted as due to static recrystallization after the main eclogite-facies deformation.

Appendix A. Electron backscatter diffraction

EBSD is a SEM technique to determine the complete lattice orientation of individual grains or subgrains with size down to 1 μm and with an absolute angular resolution of $1-2°$ (Venables and Harland, 1973; Dingley et al., 1987; Kunze et al., 1993). EBSD patterns are generated by multiple scattering of the electrons within the crystal structure and are the backscattered equivalent of the classical Kikuchi patterns observed in the TEM. The patterns consist of a series of bands, each of which corresponds to a certain lattice plane (hkl). The width of the bands is inversely related to the lattice

plane spacing and can be used, together with the angle between the bands, to index the diffraction pattern and to determine the crystallographic orientation for a known crystal lattice. Automated acquisition and analysis of EBSD patterns allows rapid measurements of a large number of points on a specimen (about 1–5 s per pattern).

EBSD patterns were collected using a SEM Cam-Scan CS44LB at ETH Zürich with an accelerating voltage of 15 kV and a beam current of approximately 2.5 nA. They were indexed using the software OIM2.0 (TSL) on a SGI Indy workstation. Orientation data of omphacite were automatically collected using an EBSD reference file of 40 reflections (Mauler et al., 1998). Rectangular sampling grids were defined to cover as much of the sections while avoiding parts of the samples that were not well polished. Orientations with a low reliability (confidence index < 0.2) were filtered out for orientation density calculations. For rutile and quartz, the electron beam was positioned manually once per individual grain and the crystallographic orientation at that point was recorded.

The number of measurements and the texture index for the three minerals omphacite, rutile and quartz are given for the studied eclogite samples in Table 1, where the grid, step size and number of total orientations refer to the automated collection of omphacite orientations. The omphacite orientations correspond to the part of the total orientations that has a high reliability (confidence index > 0.2). The fraction with a low reliability is mainly made of patterns that were collected on other mineral phases than omphacite (essentially garnet) or on surface damages.

In the gneiss samples G69 and G87, 260 resp. 280 quartz orientations were collected. The obtained texture indices for these samples were $J = 1.2$, resp. $J = 1.3$.

References

Abalos, B., 1997. Omphacite fabric variation in the Cabo Ortegal eclogite (NW Spain): relationships with strain symmetry during high-pressure deformation. J. Struct. Geol. 19 (5), 621–637.

Avé Lallemant, H.G., 1967. Structures and petrofabric analysis of an ''Alpine-type'' peridotite: the lherzolite of the French Pyrenees. Leidse Geol. Meded. 42, 1–27.

Avé Lallemant, H.G., 1978. Experimental deformation of diopside and websterite. Tectonophysics 48, 1–27.

Baker, D.W., Carter, N.L., 1972. Seismic velocity anisotropy calculated for ultramafic minerals and aggregates. Flow and fracture of rocks. The Griggs volume. Geophys. Monogr., vol. 16. Am. Geophys. Union, Washingfon, pp. 157–166.

Barruol, G., Mainprice, D., 1993. 3-D seismic velocities calculated from lattice-preferred orientation and reflectivity of a lower crustal section: examples of the Val Sesia section (Ivrea zone, northern Italy). Geophys. J. Int. 115, 1169–1188.

Bascou, J., Barruol, G., Vauchez, A., Mainprice, D., Tommasi, A., Egydio-Silva, M., 2001. Eclogite seismic properties from EBSP-derived omphacite lattice preferred orientations. Tectonophysics 342, 61–79.

Bass, J.D., 1995. Elasticity of minerals, glasses and melts. In: Ahrens, T.J. (Ed.), Mineral Physics and Crystallography: A Handbook of Physical Constants. AGU Reference Shelf, vol. 2, 53, Washington, DC.

Binns, R.A., 1967. Barroisite-bearing eclogite from Naustdal, Sogn og Fjordane, Norway. J. Petrol. 8, 349–371.

Blanchin, M.G., Faisant, P., 1979. Compression à haute température et sous atmosphère oxydante de monocristaux de rutile. Rev. Phys. Appl. 14, 619–627.

Blanchin, M.G., Fontaine, G., 1975. Transmission electron microscope observations of deformed rutile. Phys. Status Solidi A 29, 491–501.

Blanchin, M.G., Bursill, L.A., Lafage, C., 1990. Deformation and microstructure of rutile. Proc. R. Soc. London, Ser. A 429, 175–202.

Boland, J.N., Tullis, T.E., 1985. Deformation behaviour of wet and dry clinopyroxenite in the brittle to ductile transition region. Mineral and Rock Deformation: Laboratories studies. The Paterson Volume. Geophys. Monogr., vol. 36. Am. Geophys. Union, Washington, pp. 35–49.

Bouchez, J.L., Lister, G.S., Nicolas, A., 1983. Fabric asymmetry and shear sense in movement zones. Geol. Rundsch. 72 (2), 401–419.

Boudier, F., 1978. Structure and petrology of the Lanzo peridotite massif (Piemont Alps). Geol. Soc. Am. Bull. 89, 1574–1591.

Boundy, T.M., Fountain, D.M., Austrheim, H., 1992. Structural development and petrofabrics of eclogite facies shear zones, Bergen Arcs, western Norway: implications for deep crustal deformational processes. J. Metamorph. Geol. 10, 127–146.

Boyle, A.P., Prior, D.J., Banham, M.H., Timms, N.E., 1998. Plastic deformation of metamorphic pyrite: new evidence from electron-backscatter diffraction and forescatter orientation-contrast imaging. Miner. Deposita 34, 71–81.

Brenker, F.E., 1998. Mikrogefügethermochronometrie für Eklogite. PhD thesis, J.W. Goethe Universität, Frankfurt, Germany.

Brenker, F.E., Prior, D.P., Müller, W.F., 1999. Cation ordering in omphacite and effect on deformation mechanism and lattice preferred orientation. Proc. Int. Conf. Deformation Mechanisms, Rheology and Microstructures. Neustadt an der Weinstrasse, Germany, p. 11.

Buatier, M., Van Roermund, H.L.M., Drury, M.R., Lardeaux, J.M., 1991. Deformation and recrystallisation mechanisms in naturally deformed omphacites from the Sesia–Lanzo zone; geophysical consequences. Tectonophysics 195, 11–27.

Bunge, H.J., 1982. Texture Analysis in Materials Science. Butterworth, London.

Bystricky, M., 1998. High temperature deformation of clinopyrox-

ene and clinopyroxene–plagioclase aggregates. PhD thesis, Pennsylvania State University.

Bystricky, M., Mackwell, S., 2001. Creep of dry clinopyroxene aggregates. J. Geophys. Res. B106 (7), 13443–13454.

Bystricky, M., Kunze, K., Burlini, L., Burg, J.P., 2000. High shear strain of olivine aggregates: rheological and seismic consequences. Science 290, 1564–1567.

Carpenter, M.A., 1980. Composition and cation order variations in a sector-zoned blueschist pyroxene. Am. Mineral. 65, 313–320.

Carpenter, M.A., Smith, D.C., 1981. Solid solution and cation ordering limits in high temperature sodic pyroxenes from the Nybö eclogite pod, Norway. Mineral. Mag. 44, 37–44.

Carter, N.L., Baker, D.W., George, R.P., 1972. Seismic anisotropy, flow and constitution of the upper mantle, flow and fracture of rocks. The Griggs Volume. Geophys. Monogr., vol. 16. Am. Geophys. Union, Washington, pp. 167–190.

Daniel, C.G., Prior, D.J., Spear, F.S., Hirsch, D., Carlson, W., 1999. Testing the model of multiple nucleation sites for complexly zoned garnet; an application of electron backscatter diffraction and orientation contrast imaging. Abstracts with Program. Geol. Soc. Am. 31 (7), 168–169.

Dingley, D.J., Longden, M., Weinbren, J., Alderman, J., 1987. On-line analysis of electron backscatter diffraction patterns: I. Texture analysis of zone refined polysilicon. Scanning Microsc. 1, 451–456.

Dingley, D.J., Baba-Kishi, K.Z., Randle, V., 1995. Atlas of Backscattering Kikuchi Diffraction Patterns. Institute of Physics Publishing, Bristol, UK, ix-135 pp.

Engels, J.P., 1972. The catazonal poly-metamorphic rocks of Cabo Ortegal (NW Spain), a structural and petrographic study. Leidse Geol. Meded. 48 (1), 83–133.

Fliervoet, T.F., White, S.H., Drury, M.R., 1997. Evidence for dominant grain-boundary sliding deformation in greenschist- and amphibolite-grade polymineralic ultramylonites from the Redbank deformed zone, Central Australia. J. Struct. Geol. 19 (12), 1495–1520.

Fliervoet, T.F., Drury, M.R., Chopra, P.N., 1999. Crystallographic preferred orientations and misorientations in some olivine rocks deformed by diffusion or dislocation creep. Tectonophysics 303, 1–27.

Godard, G., 1981. Lambeaux probables d'une croûte océanique subductée: les éclogites de Vendée. Thèse de 3ème cycle, Université de Nantes.

Godard, G., 1983. Dispersion tectonique des éclogites de Vendée lors d'une collision continent–continent. Bull. Minéral. 106, 719–722.

Godard, G., 1988. Petrology of some eclogites in the Hercynides: the eclogites from the Southern Armorican Massif, France. In: Smith, D.C. (Ed.), Eclogites and Eclogite-Facies Rocks. Dev. Petrol., vol. 12. Elsevier, Amsterdam, pp. 451–510.

Godard, G., 2001. The Les Essarts eclogite-bearing metamorphic Complex (Vendée, Southern Armorican Massif, France). Géologie de la France. 2001 (1–2), 19–51 +2 maps.

Godard, G., Van Roermund, H.L.M., 1995. Deformation-induced clinopyroxene fabrics from eclogites. J. Struct. Geol. 17 (10), 1425–1443.

Helmstaedt, H., Anderson, D.L., Gavasci, A.T., 1972. Petrofabric studies of eclogite, spinel websterite, and spinel–lherzolite xenoliths from kimberlite–breccia pipes in southeastern Utah and northeastern Arizona. J. Geophys. Res. 77, 4350–4365.

Ingrin, J., Doukhan, N., Doukhan, J.C., 1991. High-temperature deformation of diopside single crystals: 2, Transmission electron microscopy investigation of the defect microstructures. J. Geophys. Res. 96 (B9), 14287–14297.

Ingrin, J., Doukhan, N., Doukhan, J.C., 1992. Dislocation glide systems in diopside single crystals deformed at 800–900 °C. Eur. J. Mineral. 4, 1291–1302.

Ji, S., Salisbury, M.H., Hanmer, S., 1993. Petrofabric, P-wave anisotropy and seismic reflectivity of high-grade tectonites. Tectonophysics 222, 195–226.

Kirby, S.H., Kronenberg, A.K., 1984. Deformation of clinopyroxenite: evidence for a transition in flow mechanisms and semi-brittle behaviour. J. Geophys. Res. 89 (B5), 3177–3192.

Kleinschrodt, R., McGrew, A., 2000. Garnet plasticity in the lower continental crust: implications for deformation mechanisms based on microstructures and SEM-electron channelling patterns analysis. J. Struct. Geol. 22 (6), 795–809.

Kollé, J.J., Blacic, J.D., 1983. Deformation of single-crystal clinopyroxenes: 2. Dislocation-controlled flow processes in hedenbergite. J. Geophys. Res. 88 (3), 2381–2393.

Kuijper, R.P., Vogel, D.E., Den Tex, E., 1985. Eclogite–plagiopyrigarnite relations in the catazonal complexes of Northwest Spain. Chem. Geol. 50 (1–3), 163–171.

Kumazawa, M., Helmstaedt, H., Masaki, K., 1971. Elastic properties of eclogite xenoliths from diatremes of the East Colorado Plateau and their implication to the upper mantle structure. J. Geophys. Res. 76 (5), 1231–1247.

Kunze, K., Wright, S.I., Adams, B.L., Dingley, D.J., 1993. Advances in automatic EBSP single orientation measurements. Text. Microstruct. 20, 41–54.

Kunze, K., Adams, B.L., Heidelbach, F., Wenk, H.R., 1994a. Local microstructural investigations in recrystallised quartzite using Orientation Imaging Microscopy. In: Bunge, H.J. (Ed.), Textures of Materials. DGM Informationsgesellschaft, Oberursel, Germany, pp. 1243–1250.

Kunze, K., Heidelbach, F., Wenk, H.R., Adams, B.L., 1994b. Orientation imaging microscopy of calcite rocks. In: Bunge, H.J., Siegesmund, S., Skrotski, W., Weber, K. (Eds.), Textures of Geological Materials. DGM Informationsgesellschaft, Oberursel, Germany, pp. 127–147.

Leiss, B., Barber, D.J., 1999. Mechanisms of dynamic recrystallisation in naturally deformed dolomite inferred from EBSP analyses. Tectonophysics 303, 51–69.

Lloyd, G.E., Law, R.D., Schmid, S.M., 1987. A spherical electron channelling pattern map for use in quartz petrofabric analysis: correction and verification. J. Struct. Geol. 9, 251–253.

Mainprice, D., Bouchez, J.L., Blumenfeld, P., Tubia, J.M., 1986. Dominant c-slip in naturally deformed quartz: implications for dramatic plastic softening at high temperature. Geology 14, 819–822.

Mauler, A., Kunze, K., Burg, J.P., Philippot, P., 1998. Identification of EBSD patterns in a monoclinic solid-state solution series: example of omphacite. Mater. Sci. Forum 273–275, 705–710.

Mauler, A., Bystricky, M., Kunze, K., Mackwell, S., 2000a. Micro-structures and lattice preferred orientations in experimentally deformed clinopyroxenes aggregates. J. Struct. Geol. 22 (11–12), 1633–1648.

Mauler, A., Burlini, L., Kunze, K., Burg, J.P., Philippot, P., 2000b. P-wave anisotropy in eclogites and relationship the omphacite crystallographic fabric. Phys. Chem. Earth 25 (2), 119–126.

Montigny, R., Allègre, C.J., 1974. A la recherche des océans perdus: les éclogites de Vendée, témoins métamorphisés d'une ancienne croûte océanique. C.R. Acad. Sci. Paris 279, 543–545.

Panozzo, R., 1983. Two-dimensional analysis of shape fabric using projections of digitised lines in a plane. Tectonophysics 95, 279–294.

Panozzo, R., 1984. Two-dimensional strain from the orientation of lines in a plane. J. Struct. Geol. 6, 215–221.

Peucat, J.J., Vidal, P., Godard, G., Postaire, P., 1981. Precambrian U–Pb zircon ages in eclogite and garnet–pyroxenites from South Brittany (France): an old oceanic crust in the West European Hercynian belt? Earth Planet. Sci. Lett. 60, 70–78.

Philippot, P., Van Roermund, H.L.M., 1992. Deformation processes in eclogitic rocks: evidence for the rheological delamination of the oceanic crust in deeper levels of subduction zones. J. Struct. Geol. 14, 1059–1077.

Pieri, M., Kunze, K., Burlini, L., Stretton, I.C., Olgaard, D., Burg, J.P., Wenk, R.H., 2001. Texture development in calcite through deformation and dynamic recrystallization during torsion to large strains. Tectonophysics 330 (1–2), 119–140.

Platt, J.P., 1993. Exhumation of high-pressure rocks: a review of concepts and processes. Terra Nova 5, 119–133.

Prior, D.J., Wheeler, J., 1999. Feldspar fabrics in a greenschist facies albite-rich mylonite from electron backscatter diffraction. Tectonophysics 303, 29–49.

Prior, D.J., Boyle, A.P., Brenker, F., Cheadle, M.C., Day, A., Lopez, L., Peruzzo, L., Potts, G., Reddy, S., Spiess, R., Timms, N.E., Trimby, P., Wheeler, J., Zetterstrom, L., 1999. The application of electron backscatter diffraction and orientation contrast imaging in the SEM to textural problems in rocks. Am. Mineral. 84 (11–12), 1741–1759.

Prior, D.J., Wheeler, J., Harte, B., Brenker, F., Matthews, M., 2000. Crystal plasticity of natural garnet: new microstructural evidence. Geology 28 (11), 1003–1006.

Raleigh, C.B., Talbot, J.L., 1967. Mechanical twinning in naturally and experimentally deformed diopside. Am. J. Sci. 265, 151–165.

Raterron, P., Doukhan, N., Jaoul, O., Doukhan, J.C., 1994. High temperature deformation of diopside: IV. Predominance of {110} glide above 1000 °C. Phys. Earth Planet. Int. 82, 209–222.

Rossi, G., 1988. A review of the crystal-chemistry of clinopyroxenes in eclogites and other high-pressure rocks. In: Smith, D.C. (Ed.), Eclogites and Eclogite-Facies Rocks. Dev. Petrol., vol. 12. Elsevier, Amsterdam, pp. 237–270.

Schmid, S.M., 1982. Microfabric studies as indicators of deformation mechanisms and flow laws operative in mountain building. In: Hsu, K.J. (Ed.), Mountain Building Processes. Academic Press, London, pp. 95–110.

Schmid, S.M., Casey, M., 1986. Complete fabrics analysis of some commonly observed quartz *c*-axis patterns. In: Hobbs, B.E., Heard, H.C. (Eds.), Mineral and Rock Deformation: Laboratory Studies. The Paterson Volume. Geophys. Monogr., vol. 36. Am. Geophys. Union, Washington, pp. 161–199.

Siegesmund, S., Takeshita, T., Kern, H., 1989. Anisotropy of Vp and Vs in an amphibolite of the deeper crust and its relationship to the mineralogical, microstructural and textural characteristics of the rock. Tectonophysics 257, 25–38.

Spiess, R., Peruzzo, L., Prior, D.J., Wheeler, J., 2001. Development of garnet porphyroblasts by multiple nucleation, coalescence and boundary misorientation driven rotations. J. Metamorph. Petrol. 19, 269–290.

Van Panhuis-Sigler, M., Hartman, P., 1981. Morphologie théorique de certains pyroxènes déduite de la structure cristalline. Bull. Minéral. 104, 95–106.

Van Roermund, H.L.M., 1992. Thermal and deformation induced omphacite microstructures from eclogites; implications for the formation and uplift of HP metamorphic terrains. Recent Trends Mineral., vol. 1. Int. Research Council, pp. 117–151.

Van Roermund, H.L.M., Boland, J.N., 1983. Retrograde *P–T* trajectories of high temperature eclogites deduced from omphacite exsolution microstructures. Bull. Mineral. 106, 723–726.

Venables, J.A., Harland, C.J., 1973. Electron back-scattering patterns — a new technique for obtaining crystallographic information in the scanning electron microscope. Philos. Mag. 27, 1193–1200.

Vollmer, F.W., 1990. An application of eigenvalue methods to structural strain domain analysis. Bull. Geol. Soc. Am. 102, 786–791.

Weber, U., 1997. Mikrostrukturen und Texturen in natürlich deformiertem Eklogit: Entwicklung und Anwendung neuer Techniken mit dem Rasterelektronen-mikroskop. Diploma thesis, Justus-Liebig-Universität, Giessen, Germany.

Wenk, H.R., Matthies, S., Donovan, J., Chateigner, D., 1998. BEARTEX: a Windows-based program system for quantitative texture analysis. J. Appl. Crystal. 31, 262–269.

Woodcock, N.H., 1977. Signification of fabric shapes using an eigenvalues method. Bull. Geol. Soc. Am. 88, 1231–1236.